LETTER Communicated by Carson Chow

Dynamics of Deterministic and Stochastic Paired Excitatory–Inhibitory Delayed Feedback

Carlo R. Laing
c.r.laing@massey.ac.nz
André Longtin
alongtin@physics.uottawa.ca
Department of Physics, University of Ottawa, Ottawa, Canada K1N 6N5

We examine the effects of paired delayed excitatory and inhibitory feedback on a single integrate–and–fire neuron with reversal potentials embedded within a feedback network. These effects are studied using bifurcation theory and numerical analysis. The feedback occurs through modulation of the excitatory and inhibitory conductances by the previous firing history of the neuron; as a consequence, the feedback also modifies the membrane time constant. Such paired feedback is ubiquitous in the nervous system. We assume that the feedback dynamics are slower than the membrane time constant, which leads to a rate model formulation. Our article provides an extensive analysis of the possible dynamical behaviors of such simple yet realistic neural loops as a function of the balance between positive and negative feedback, with and without noise, and offers insight into the potential behaviors such loops can exhibit in response to time-varying external inputs. With excitatory feedback, the system can be quiescent, can be periodically firing, or can exhibit bistability between these two states. With inhibitory feedback, quiescence, oscillatory firing rates, and bistability between constant and oscillatory firing-rate solutions are possible. The general case of paired feedback exhibits a blend of the behaviors seen in the extreme cases and can produce chaotic firing. We further derive a condition for a dynamically balanced paired feedback in which there is neither bistability nor oscillations. We also show how a biophysically plausible smoothing of the firing function by noise can modify the existence and stability of fixed points and oscillations of the system. We take advantage in our mathematical analysis of the existence of an invariant manifold, which reduces the dimensionality of the dynamics, and prove the stability of this manifold. The novel computational challenges involved in analyzing such dynamics with and without noise are also described. Our results demonstrate that a paired delayed feedback loop can act as a sophisticated computational unit, capable of switching between a variety of behaviors depending on the input current, the relative strengths and asymmetry of the two parallel feedback pathways, and the delay distributions and noise level.

Neural Computation **15, 2779–2822** (2003)

1 Introduction

Feedback is ubiquitous in both the central and peripheral nervous systems (Cajal, 1909). From simple reflex arcs in the spinal cord to sensory information processing, feature extraction, attention, and motor control, feedback circuitry is involved. Feedback loops can occur in isolation, in series, in parallel, or even in nested configurations. Their activity can be modulated by external input, and in turn they can modulate the activity of other neural circuits. The delay time for feedback activity to circulate around a loop can vary considerably from milliseconds to hundreds of milliseconds, depending on axonal propagation delays, synaptic kinetics, dendritic integration, and the integration and latency of the firing mechanism.

In many cases, the feedback activity is a significant component of the total conductance of the cell (Berman & Maler, 1999). It can thus affect the membrane time constant and the input integration properties of the cell (Nelson, 1994). Experimental and modeling studies of recurrent loops in neurophysiology include analyses of feedback between the thalamus and the cortex (see, e.g., Contreras, Destexhe, Sejnowski, & Steriade, 1996; Destexhe, 1994; Murphy, Duckett, & Sillito, 1999), between the different areas of visual cortex (Crick & Koch, 1998), within the hippocampus (Traub & Miles, 1991; Ermentrout & Kopell, 1998), and in the electrosensory system (Berman & Maler, 1999; Doiron, Chacron, Maler, Longtin, & Bastian, 2003).

Our article concerns the mathematical analysis of the activity of a neuron embedded in a paired feedback network, which is common and defined as follows. The neuron of interest projects to a population of cells, and these in turn project back to it (and its neighbors, to which it is very weakly coupled) via both inhibitory and excitatory recurrent connections. Each feedback pathway is assumed to have its own distribution of delays and minimal delay, but is driven by the same firing activity: that of our neuron of interest. We wish to understand the dynamics of this paired feedback system, as well as the effect of noise on these dynamics. Our analysis will first consider separately the effects of negative (inhibitory) and positive (excitatory) feedback, and then study the dynamics as a function of the balance between (or relative strength of) these two kinds of feedback. We assume throughout our work that the feedback activity is in the form of a rate rather than spikes and that it produces currents via conductance changes at synapses with reversal potentials.

Our main motivation is to understand the kinds of behaviors exhibited by these nets, from which one can record experimentally under a variety of stimulus conditions and isolate the effect of various feedback loops (Doiron et al., 2003; Murphy et al., 1999). Much of the inspiration comes from the known feedback circuitry in the electrosensory pathways of the weakly electric fish *Apteronotus leptorhynchus* (Bastian, 1990; Nelson, 1994; Berman

& Maler, 1999), which combines recurrent excitation and inhibition in the paired manner described above (the so-called direct pathway). Such paired loops are spatially localized, are in fact arranged in parallel, and are also in parallel within global paired and spatially diffuse feedback circuitry; it is also clear that these loops are nested within other ones involving other nuclei.

Recurrent inhibitory feedback or "negative feedback" has received much attention due to its involvement in regulatory control (Stark, 1968; Glass & Mackey, 1988; Longtin & Milton, 1989), adaptation (Fohlmeister, 1979; Ermentrout, Pascal, & Gutkin, 2001), hippocampal circuitry (Traub & Miles, 1991; Mackey & an der Heiden, 1982; Eurich, Mackey, & Schwegler, 2002), and spike pattern generation (Diez-Martinez & Segundo, 1983; Foss & Milton, 2000). Recurrent excitation or "positive feedback" has also been studied in many contexts, such as spike pattern generation (Pakdaman, Vibert, Boussard, & Azmy, 1996) and the multistability in the activity of neocortical circuits (Douglas, Koch, Mahowald, Martin, & Suarez, 1995; Hahnloser, Sarpeshkar, Mahowald, Douglas, & Seung, 2000). There have also been studies of so-called mixed feedback in which the feedback can be either positive or negative depending on the current state of the firing activity. Such feedback can give rise to regular and irregular patterns of firing activity (Mackey & an der Heiden, 1982; Glass & Mackey, 1988; Longtin & Milton, 1988; Glass & Malta, 1990). It is also known generally that reciprocally coupled populations of excitatory and inhibitory neurons can exhibit oscillatory activity even in the absence of delays (see, e.g., Dayan & Abbott, 2001); in fact, the early work of Wilson and Cowan (1972) showed that feedback excitation without delays can lead to bistability in firing rates and that feedback inhibition without delay can lead to oscillations in the firing rates. Reciprocally connected excitatory and inhibitory neurons with more biophysical detail display similar features as well as other interesting switches to bursting or low-frequency firing (Latham, Richmond, Nelson, & Nirenberg, 2000), can exhibit chaos (Hansel & Sompolinsky, 1992), and can even support the propagation of slow pulses in the presence of delays (Golomb & Ermentrout, 2002).

The relevance of delayed feedback or feedback with slow synapses has further been shown in the context of memory and learning in real neurons (Ernst, Pawelzik, & Geisel, 1995; Brunel, 1996; Kistler & van Hemmen, 1999; Knight 2000; Seung, Lee, Reis, & Tank, 2000) and artificial neural networks (Sompolinsky & Kanter, 1986; Marcus & Westerwelt, 1989; Herz, Li, & van Hemmen, 1991). Some progress has even been made on the analysis of delayed recurrent networks with noise for learning (Herz et al., 1991; Brunel, 1996) and working memory (Wang, 1999). Delayed feedback has also been studied in some detail in the context of coupled neural oscillators and of nonneural excitable systems as well (see, e.g., Kunysz, Shrier, &

Glass, 1997). Plant (1981) was a pioneer in this area, analyzing the dynamics of the FitzHugh-Nagumo neuron model with delayed positive or negative self-feedback. More recently, Giannakopoulos and Zapp (2001) considered one inhibitory and one excitatory neuron, coupled to each other and themselves, with delay; from the point of view of the excitatory neuron, this loop provides delayed inhibitory feedback. There have also been analyses of delay-induced oscillations and frustrations in neural nets with delays (Belair, Campbell, & van den Driessche, 1996), as well as of multistability in nets with single delays (Foss, Longtin, Mensour, & Milton, 1996), multiple delays (Shayer & Campbell, 2000) or multiple loops (Campbell 1999; Glass & Malta, 1990). Traveling waves in pulse-coupled integrate-and-fire neurons with delays have been found by Bressloff and Coombes (1999). The same authors have also found that rhythmic bursting patterns can occur in asymmetric networks of linear integrate-and-fire neurons with additive synaptic inputs (i.e., without reversal potentials), when there was a mixture of inhibitory and excitatory synaptic coupling (Bressloff & Coombes, 2000a).

Despite all these studies, delayed paired feedback, especially in the presence of noise, has not received much attention from the dynamical point of view, even though it is frequently encountered (Crick & Koch, 1998; Murphy et al., 1999; Berman & Maler, 1999; Hahnloser et al., 2000). Here we combine both delayed feedback with the ability to change independently the strengths of the excitatory and inhibitory components of the feedback in the context of a neuron embedded in a network. These feedbacks can have different properties, such as different strengths, integration and synaptic timescales, and propagation delays. Recurrent excitation and inhibition, and as we will see under certain conditions, mixed feedback are special cases of this paired feedback.

Our article provides a general framework for analyzing paired feedback with delays and noise due, for example, to synaptic activity. It reveals that as a whole, the paired feedback loop forms a sophisticated computational unit in comparison with a single neuron due to the wide variety of firing patterns it can exhibit. This is true even if the dynamics of the neuron at its core are of the simple leaky integrate-and-fire type. As feedback loops are often arranged in series or parallel configurations, they can be seen as forming networks of coupled interacting elements that in turn perform perhaps more sophisticated computations. A first step toward understanding or designing such networks in vivo or in silico is to fully analyze the dynamics of a general paired delayed feedback loop, as we do here. Our work ultimately provides a formalism to analyze the activity in deterministic and stochastic neural feedback loops as a function of model parameters, such as strength of feedback and the distribution of propagation and activation delays involved in each path.

The article is organized as follows. Section 2 derives the generic model of neural delayed feedback used throughout our work. The constant equilibria (fixed points) of this model are analyzed in section 3. The dynamics of the

model for the simplest kind of feedback kernel (exponential) with a fixed minimal delay are analyzed in section 4, first for excitatory feedback alone and then inhibitory feedback alone, then by smoothly varying the feedback from one case to the other. The possible chaotic solutions in this case are also presented in this section. The next simplest case in which the delay kernel exhibits a maximum later than the minimal delay is then analyzed in section 5. In this case, the strongest determinant of the firing dynamics is not the minimal delay but rather some time earlier in the past. As in section 4, results are presented first for excitatory and inhibitory feedback alone and then for paired feedback. Section 6 extends the results to kernels whose localization in time can be arbitrarily narrow (the extreme case corresponds to a delta function at a lag equal to the minimal delay plus another fixed delay). Departures from the symmetric cases of equal delays and feedback kernel (i.e., memory) decay rates are briefly analyzed in section 7 for exponential and higher-order kernels. The influence of noise on the behavior of the paired feedback loop is then analyzed using a biophysically plausible model in section 8. A conclusion and a look at future problems completes the letter in section 9. Our bifurcation analysis in sections 4 and beyond is supplemented by DDE-BIFTOOL, a public domain Matlab package for the bifurcation analysis of smooth delay-differential equations.

2 Model

In our model, a neuron in population 1 (from which one can record) projects to neurons in population 2, which in turn project back excitatorily and inhibitorily to neurons in population 1 (the inhibition typically arises from interneurons). The neurons in population 1 are weakly coupled in the case of the electric fish (Berman & Maler, 1999), so this coupling is neglected in our study. We further take into account the fact that there is a minimal time for neural activity to propagate around a neural loop, which brings a finite minimal delay into the problem. Beyond this minimal delay, there is an extra time delay that follows some distribution. For example, in the weakly electric fish *Apteronotus leptorhynchus*, the positive and negative feedback loops starting from an electrosensory lateral line lobe (ELL) pyramidal cell, projecting to the Pd nucleus and subsequently back to the ELL, involve a minimal delay of about 12 msec, plus a distribution of delays with a mean of around 13 msec as well; thus, there is a mean delay of approximately 25 msec (Berman & Maler, 1999; Doiron et al., 2003). Thus, the excitatory and inhibitory feedback activities to the neuron of interest in population 1 are a function of its past firing activity. This is the general generic case that we study; the specifics of the distribution of delays, such as the minimal time and width of the distribution, will vary from case to case. The relative strengths of the two feedbacks can depend on the temporal properties of the input from primary sensory neurons and other factors. In our study, the dynamics of the paired feedback is investigated as a function of the balance

between the loops (i.e., their relative strengths), regardless of the cause of this balance, and as a function of the input (nonfeedback) bias current.

The neuron model we use at the core of the feedback loop is a leaky integrate–and–fire neuron with reversal potentials whose governing equation is

$$C\frac{dV}{dt} = I + g_L(V_L - V) + g_e(V_e - V) + g_i(V_i - V) \tag{2.1}$$

with reset and threshold values V_r and V_θ, respectively; that is, if $V(t^-) = V_\theta$, then $V(t^+) = V_r$. C is the capacitance, I is the input current, and g_L, g_e, and g_i are the leak, excitatory, and inhibitory conductances, respectively. V_L is the leak potential, and V_e and V_i are the excitatory and inhibitory reversal potentials, respectively. We assume that there is an absolute refractory period τ_r—that $V = V_r$ for a time τ_r after each firing. The instantaneous firing rate of model 2.1 is

$$f(t) \approx H(V_{ss}(t) - V_\theta)\left\{\tau_r - \frac{C}{g_{tot}(t)}\ln\left[\frac{V_\theta - V_{ss}(t)}{V_r - V_{ss}(t)}\right]\right\}^{-1}, \tag{2.2}$$

where H is the Heaviside function,

$$g_{tot}(t) = g_L + g_e(t) + g_i(t) \tag{2.3}$$

and

$$g_{tot}(t)V_{ss}(t) = g_L V_L + g_e(t)V_e + g_i(t)V_i + I. \tag{2.4}$$

This approximation for the firing rate is due to the fact that an equality in equation 2.2 is appropriate only if all quantities in equation 2.1 are constant (apart from the voltage). Here, however, we assume that the conductances g_e and g_i are functions of time, since they are affected by feedback activity (see below). This activity is also assumed to vary on a timescale slower than the membrane time constant in the leaky integrate-and-fire (LIF) model. The timescale of the feedback activity is a function of both the response properties of the population 2 cells (Pd nucleus in the case of weakly electric fish, of V1 neurons in the case of the visual system which project back to LGN neurons) and the feedback synapses. Since the total conductance, and thus the membrane conductance, depends on the feedback input, this assumption is all the more justified the stronger the feedback activity is. This assumption of relative slowness will allow us to directly use the deterministic firing function of our model, equation 2.2, in a rate description, as done in other contexts (Ermentrout, 1994; Bressloff & Coombes, 2000b; and Hansel & Mato, 2001, for the quadratic integrate-and-fire model).

To implement feedback in the model, equation 2.1, we assume that the excitatory and inhibitory conductances depend on the firing frequency of the neuron at times in the past. Specifically, we write g_e and g_i as

$$g_e(t) = \beta_e \int_{-\infty}^{t-\tau_e} G_e^{m_e}(t-s) f(s)\, ds \tag{2.5}$$

$$g_i(t) = \beta_i \int_{-\infty}^{t-\tau_i} G_i^{m_i}(t-s) f(s)\, ds, \tag{2.6}$$

where the feedback kernels G_e and G_i are described below. We are assuming here a homogeneous population of neurons that communicate mainly via feedback (directly or via another population), and the firing function $f(t)$ drives this feedback activity. This function f can be seen as the population instantaneous rate under asynchronous conditions, obtained by summing all spike trains from all the cells. Since all cells are identical as a first approximation, they all receive the same time-dependent synaptic input, and each of their behaviors is governed by equations 2.5 and 2.6 in conjunction with equation 2.2. The feedback gains β_e, β_i account among other things for the number of neurons summing their output. The firing frequency, equation 2.2, is thus a good approximation to the population instantaneous rate for slowly varying inputs.

The feedback kernels are chosen as

$$G_e^{m_e}(t) = \begin{cases} \frac{a_e^{m_e+1}}{m_e!}(t-\tau_e)^{m_e} \exp\left[-a_e(t-\tau_e)\right] & \text{if } \tau_e < t \\ 0 & \text{if } \tau_e > t \end{cases} \tag{2.7}$$

and

$$G_i^{m_i}(t) = \begin{cases} \frac{a_i^{m_i+1}}{m_i!}(t-\tau_i)^{m_i} \exp\left[-a_i(t-\tau_i)\right] & \text{if } \tau_i < t \\ 0 & \text{if } \tau_i > t. \end{cases} \tag{2.8}$$

The function $G_e^{m_e}(t)$ is zero until time τ_e, after which it rises to a maximum before decaying back to zero from above. τ_e (and also τ_i below) represents the minimal delay for activity to propagate around the loop. This value can be set to zero in our formalism, as is often done in modeling neural circuitry and neural networks, but our analysis is valid for any (zero or positive) τ_e and τ_i. Note that the total mean delay is $\tau_{e,i} + (m_{e,i}+1)/a_{e,i}$. Thus, $g_e(t)$ is a scaled convolution of the firing frequency $f(t)$ in the past with the convolution kernel $G_e^{m_e}(t)$. This convolution smoothes $f(t)$ and is meant to mimic the effect of the output of the neuron exciting another cell or collection of cells, which then project back in a paired fashion to the neuron under study. Note that $g_e(t)$ depends on f only at times earlier than $t - \tau_e$. Similar statements hold for $g_i(t)$. The coefficients β_e and β_i are the nonnegative strengths of the excitatory and inhibitory feedback, respectively. In practical situations, τ_i is

often greater than τ_e, since the inhibitory feedback loop is often formed by excitatory feedback returning not only to the neuron but impinging as well on an interneuron that inhibits the neuron. The inhibitory loop can thus include extra axonal and synaptic delay times. As inhibitory loops can also exist independently from excitatory ones, our results are developed for the general case that does not assume an ordering of τ_e and τ_i.

Because of the form of the convolution kernels 2.7 and 2.8, we can derive a recursive formula for their derivatives (an der Heiden, 1980). The derivative of equation 2.7 when $\tau_e < t$ is

$$\frac{a_e^{m_e+1}}{(m_e-1)!}(t-\tau_e)^{m_e-1}\exp\left[-a_e(t-\tau_e)\right] - \frac{a_e^{m_e+2}}{m_e!}(t-\tau_e)^{m_e}\exp\left[-a_e(t-\tau_e)\right], \tag{2.9}$$

so we can write

$$[G_e^{m_e}]'(t) = a_e G_e^{m_e-1}(t) - a_e G_e^{m_e}(t) \tag{2.10}$$

This is true for all integer $m_e > 1$. Thus, differentiating equation 2.5, we obtain

$$\frac{dg_e}{dt} = \beta_e \int_{-\infty}^{t-\tau_e} [G_e^{m_e}]'(t-s) f(s)\, ds = \beta_e \int_{-\infty}^{t-\tau_e} [a_e G_e^{m_e-1}(t-s) - a_e G_e^{m_e}(t-s)] f(s)\, ds. \tag{2.11}$$

Defining

$$y_{m_e-1}(t) \equiv \int_{-\infty}^{t-\tau_e} G_e^{m_e-1}(t-s) f(s)\, ds \tag{2.12}$$

and using equation 2.5, we can write equation 2.11 as

$$\frac{dg_e}{dt} = a_e[\beta_e y_{m_e-1} - g_e]. \tag{2.13}$$

Differentiating equation 2.12 and using equation 2.10, we obtain

$$\frac{dy_{m_e-1}}{dt} = \int_{-\infty}^{t-\tau_e} [G_e^{m_e-1}]'(t-s) f(s)\, ds \tag{2.14}$$

$$= \int_{-\infty}^{t-\tau_e} [a_e G_e^{m_e-2}(t-s) - a_e G_e^{m_e-1}(t-s)] f(s)\, ds \tag{2.15}$$

$$= a_e[y_{m_e-2}(t) - y_{m_e-1}(t)] \tag{2.16}$$

if $m_e > 1$. This process can be repeated for y_{m_e-2} and so on, and terminates when $m_e = 1$. In this case, we have

$$y_0(t) = \int_{-\infty}^{t-\tau_e} a_e \exp\left[-a_e(t-s-\tau_e)\right] f(s)\, ds, \tag{2.17}$$

so that

$$\begin{aligned}\frac{dy_0}{dt} &= -a_e \int_{-\infty}^{t-\tau_e} a_e \exp\left[-a_e(t-s-\tau_e)\right] f(s)\, ds + a_e f(t-\tau_e) \\ &= a_e[f(t-\tau_e) - y_0(t)].\end{aligned} \tag{2.18}$$

Thus, combining equations 2.13 and 2.16 for $m_e > 1$ and equation 2.18, we have $m_e + 1$ equations:

$$\frac{dg_e}{dt} = a_e[\beta_e y_{m_e-1} - g_e] \tag{2.19}$$

$$\frac{dy_{m_e-1}}{dt} = a_e[y_{m_e-2} - y_{m_e-1}] \tag{2.20}$$

$$\vdots$$

$$\frac{dy_1}{dt} = a_e[y_0 - y_1] \tag{2.21}$$

$$\frac{dy_0}{dt} = a_e[f(t-\tau_e) - y_0], \tag{2.22}$$

where, if not indicated, the variables on the right-hand sides are evaluated at time t. A similar process can be undertaken for g_i, resulting in a further $m_i + 1$ equations:

$$\frac{dg_i}{dt} = a_i[\beta_i z_{m_i-1} - g_i] \tag{2.23}$$

$$\frac{dz_{m_i-1}}{dt} = a_i[z_{m_i-2} - z_{m_i-1}] \tag{2.24}$$

$$\vdots$$

$$\frac{dz_1}{dt} = a_i[z_0 - z_1] \tag{2.25}$$

$$\frac{dz_0}{dt} = a_i[f(t-\tau_i) - z_0]. \tag{2.26}$$

Equations 2.5 and 2.6 are integral equations relating the conductances $g_e(t)$ and $g_i(t)$ to $f(t)$. Because of the form of $G_e^{m_e}$ and $G_i^{m_i}$, we have been able to derive a set of equivalent delay differential equations that govern the dynamics of $g_e(t)$ and $g_i(t)$. Recalling that $f(t)$ is a function of $g_e(t)$ and $g_i(t)$

through equation 2.2, equations 2.19 through 2.26 form a closed system. They will be a valid description of the dynamics of equations 2.1, 2.5, and 2.6, provided the spiking dynamics of the neuron occur on a fast timescale relative to the timescale of the feedback delay and of the time evolution of the conductances associated with the feedback activity.

One way to think of equations 2.19 through 2.22 is that y_0 is a low–pass filtered version of $f(t-\tau_e)$, y_i is a low–pass filtered version of y_{i-1} for $i = 1, \ldots, m_e - 1$, and g_e is a low–pass filtered version of y_{m_e-1}, with strength β_e. The delayed quantity $g_e(t-\tau_e)$ is then used in determining $f(t-\tau_e)$ via equations 2.2 and 2.4. Equations 2.23 through 2.26 can be interpreted in a similar way. We now consider the fixed points of 2.19 through 2.26.

3 Fixed Points

We first analyze the equilibria of our model dynamical system. This can be done in the general case of arbitrary parameters. At a fixed point of equations 2.19 through 2.26, the frequency f is no longer a function of time, so let us write equation 2.2 as

$$f(g_e, g_i) = H(V_{ss} - V_\theta)\left\{\tau_r - \frac{C}{g_{tot}} \ln\left[\frac{V_\theta - V_{ss}}{V_r - V_{ss}}\right]\right\}^{-1}, \tag{3.1}$$

where g_{tot} and V_{ss} are given by the time–independent versions of equations 2.3 and 2.4, respectively. From equations 2.19 through 2.21, we see that

$$g_e = \beta_e y_{m_e-1} \quad \text{and} \quad y_{m_e-1} = y_{m_e-2} = \cdots = y_0 \equiv y \tag{3.2}$$

at a fixed point, and from equations 2.23 through 2.25 that

$$g_i = \beta_i z_{m_i-1} \quad \text{and} \quad z_{m_i-1} = z_{m_i-2} = \cdots = z_0 \equiv z. \tag{3.3}$$

From equations 2.22 and 2.26, we see that

$$y = f(\beta_e y, \beta_i z) \quad \text{and} \quad z = f(\beta_e y, \beta_i z), \tag{3.4}$$

that is, $y = z$, so to find fixed points of the system 2.19 through 2.26, we need only find the roots of

$$y = f(\beta_e y, \beta_i y), \tag{3.5}$$

where $f(g_e, g_i)$ is given by equation 3.1. If y^* is a root of equation 3.5, then the fixed point for the system 2.19 through 2.26 is of the form

$$\begin{aligned}&[g_e, y_{m_e-1}, \ldots, y_0, g_i, z_{m_i-1}, \ldots, z_0] \\ &\quad = [\beta_e y^*, y^*, \ldots, y^*, \beta_i y^*, y^*, \ldots, y^*].\end{aligned} \tag{3.6}$$

Note that the fixed points of equations 2.19 through 2.26 do not depend on τ_e, τ_i, a_e, or a_i. This is to be expected, as these parameters affect only the time course of the convolution kernels 2.7 and 2.8.

4 Exponential Kernels ($m = 0$)

We now consider a simple case of exponential feedback kernels G_e and G_i, corresponding to the $m = 0$ case. We will analyze this case first for excitatory feedback alone, then inhibitory feedback alone, then with paired feedback (both excitatory and inhibitory). The results will be discussed as a function of the balance between the two kinds of feedback. Our analysis will allow us to smoothly connect the dynamics in the two limiting cases. We choose $\tau_e = \tau_i \equiv \tau$ and $a_e = a_i = a$ for simplicity; asymmetric cases are discussed in section 7. The convolution kernels are

$$G_e(t) = G_i(t) = \begin{cases} a \exp\left[-a(t-\tau)\right] & \text{if } \tau < t \\ 0 & \text{if } t < \tau. \end{cases} \tag{4.1}$$

This means that, for $m = 0$, the memory of the past decays exponentially. Note, however, that there still is a minimal delay τ, so we expect delay-differential dynamics even in this simplest $m = 0$ case. The delayed dynamics simply become ordinary differential equations when the physiological situation dictates that this minimal delay can be neglected (i.e., $\tau = 0$). Substituting these expressions for $G_e(t)$ and $G_i(t)$ into equations 2.5 and 2.6 and differentiating with respect to time, we obtain

$$\frac{dg_e(t)}{dt} = a[\beta_e f(g_e(t-\tau), g_i(t-\tau)) - g_e(t)] \tag{4.2}$$

$$\frac{dg_i(t)}{dt} = a[\beta_i f(g_e(t-\tau), g_i(t-\tau)) - g_i(t)]. \tag{4.3}$$

Note that we can rescale time in equations 4.2 and 4.3 so that either $a = 1$ or $\tau = 1$. From now until specified below, we assume that time has been rescaled so that $a = 1$.

If neither β_e nor β_i is zero, we see that

$$\frac{d}{dt}\left(\frac{\beta_e g_i}{\beta_i} - g_e\right) = -\left(\frac{\beta_e g_i}{\beta_i} - g_e\right); \tag{4.4}$$

that is, the difference between g_e and $\beta_e g_i/\beta_i$ decays exponentially in time to zero, and thus the line $g_e = \beta_e g_i/\beta_i$ is attracting. It is also invariant, since on this line (using equation 4.3),

$$\frac{dg_e}{dt} = \frac{\beta_e}{\beta_i}\frac{dg_i}{dt} \tag{4.5}$$

$$= \frac{\beta_e}{\beta_i}[\beta_i f(g_e(t-\tau), g_i(t-\tau)) - g_i(t)] \tag{4.6}$$

$$= \beta_e f(g_e(t-\tau), g_i(t-\tau)) - g_e(t), \tag{4.7}$$

which is just equation 4.2. Thus when $\beta_i \neq 0$, the attractor of the system 4.2 and 4.3 with paired feedback lies on the line $g_e = \beta_e g_i/\beta_i$ and is governed by the single delay differential equation,

$$\frac{dg_i(t)}{dt} = \beta_i f(\beta_e g_i(t-\tau)/\beta_i, g_i(t-\tau)) - g_i(t). \tag{4.8}$$

If $\beta_i = 0$, we have the single equation,

$$\frac{dg_e(t)}{dt} = \beta_e f(g_e(t-\tau), 0) - g_e(t). \tag{4.9}$$

The stability of this invariant manifold for the $m = 1$ and for the $m > 1$ cases will be proved in theorems 1 and 3, respectively.

4.1 Excitatory Feedback Only. We first consider the case of only excitatory feedback; we set $\beta_i = 0$. Fixed points of equation 4.9 satisfy

$$g = \beta_e f(g, 0). \tag{4.10}$$

Below we will denote such fixed points by $\hat{g}$. For each value of I, $f(g, 0)$ is zero for $g < [g_L(V_L - V_\theta) + I]/(V_\theta - V_e)$ and monotonically rises from zero as g is increased past this value. Since $V_\theta - V_e < 0$, increasing I decreases the value of g at which $f(g, 0)$ switches from being zero to being nonzero. When $f(g, 0)$ is nonzero, it is concave down. These properties imply that equation 4.10 may have more than one solution, depending on the value of I.

For the rest of the article we use the typical parameter set shown in Table 1. Note that τ_r is the absolute refractory period, not a delay, even though it acts as a delay. Its effect is taken into account directly by its inclusion in the firing function, equation 2.2. We see that $g = 0$ is always a solution of equation 4.10 (for which the firing frequency is zero) when $(I + g_L V_L)/g_L < V_\theta$. For the parameters above, this is equivalent to $I < I_c \equiv 0.6$. As suggested above, the presence of excitatory feedback means that equation 4.10 may have more than one solution. In particular, it may have nonzero solutions when I is less than I_c. This is shown in Figure 1, where we plot f as a function of I for

Table 1: Model Parameters.

C	g_L	V_i	V_L	V_r	V_θ	V_e	τ_r
1	0.5	−0.3	−0.2	0	1	1.2	0.05

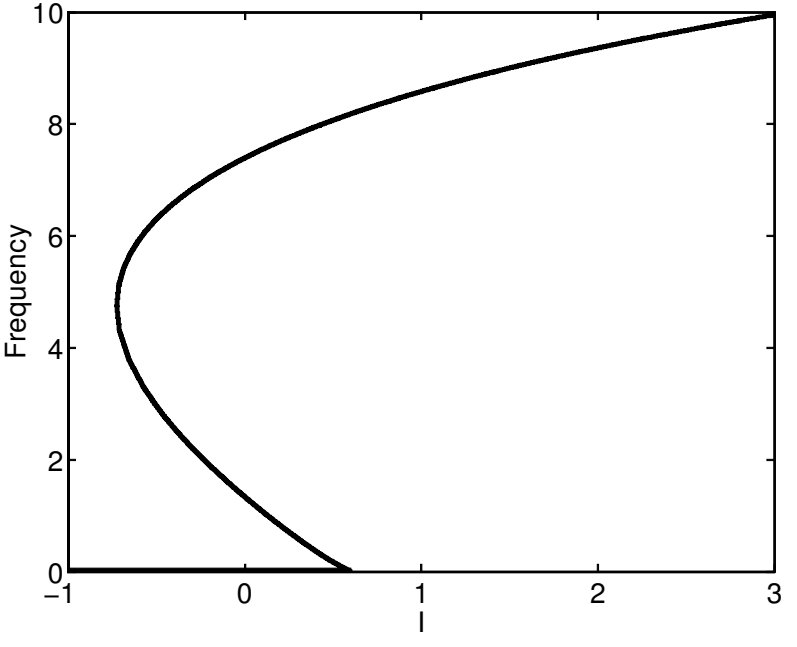

Figure 1: Dynamics of excitatory delayed feedback. Firing frequency as a function of I for equation 4.9 for $\beta_i = 0, \beta_e = 3$. Other parameters are given in Table 1. The upper branch is stable, the middle branch unstable, and the zero solution that exists for $I < 0.6$ is stable. The frequency is bounded from above by $1/\tau_r$. Here $\tau_e = 1$.

the parameter values $\beta_i = 0$, $\beta_e = 3$. We see that for $-0.75 < I < 0.6$, equation 4.10 has three solutions, two of which are nonzero. The two nonzero solutions are destroyed in a saddle–node bifurcation as I decreases through ~ -0.75. In Figure 2, we show the results of following this bifurcation in the β_e, I plane (β_e is the strength of the excitatory feedback). We see that as β_e is increased, the range of I values over which there is bistability increases. This bistability disappears when the feedback strength goes to zero, as expected from our knowledge of leaky integrate-and-fire dynamics. Further, as β_e increases, nonzero frequency fixed points can exist for lower and lower values of I as compared to the case without feedback.

4.1.1 Stability. We now investigate the stability of the fixed points of equation 4.9. Its linearization about a fixed point $\hat{g}$ is

$$\frac{dx}{dt} = \beta_e d_1 x(t - \tau) - x(t), \tag{4.11}$$

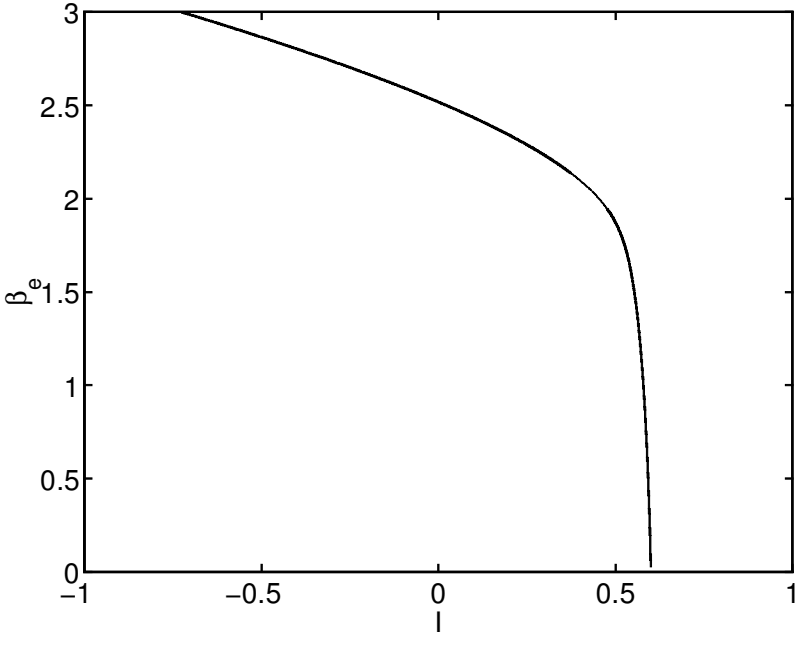

Figure 2: The curve of saddle-node bifurcations of fixed points of equation 4.9 for $\beta_i = 0$ (recurrent excitation only). Other parameters are given in Table 1. There is also a curve of bifurcations of fixed points along the line $I = I_c = 0.6$, corresponding to the annihilation of the zero fixed point (see Figure 1). Thus, the horizontal distance between the curve and the $I = I_c$ curve is a measure of the width of the bistability region. This width grows with β_e.

where $x = g_e - \hat{g}$, and d_1 is the derivative of f with respect to its first argument, evaluated at $(g_e, g_i) = (\hat{g}, 0)$. Note that d_1 is nonnegative. Defining $A \equiv \beta_e d_1$ and looking for solutions of the form $x = Be^{\lambda t}$ for some constant B, we find that λ satisfies

$$\lambda + 1 = Ae^{-\lambda\tau}. \tag{4.12}$$

We have the following well–known theorem regarding the roots of equation 4.12, which we state without proof (Guglielmi & Hairer, 1999; Hayes, 1950; Stépán, 1989).

If and only if $A < 1$ and

$$\tau < \frac{\cos^{-1}(1/A)}{\sqrt{A^2 - 1}}, \tag{4.13}$$

then all roots of equation 4.12 have negative real part, and the fixed point $\hat{g}$ of equation 4.9 is asymptotically stable.

By plotting $\beta_e f(g, 0)$ as a function of g for various values of I, it is clear that the frequency as a function of I must look like Figure 1, at least for β_e small enough. It is also clear that $0 < A = \beta_e d_1 < 1$ for points on the upper branch of solutions, so these will always be stable. Similarly, $A = 0$ for the zero solution, when it exists, and $1 < A$ for the middle branch. Thus, excitatory feedback produces the possibility of multistability and of firing for $I < I_c$, as shown in Figure 1. A similar result for a sigmoidal function f was shown by an der Heiden (1980). In summary, the dominant feature of purely excitatory feedback with a minimal delay and exponentially decaying memory beyond this delay is bistability between a quiescent state and a periodically firing state.

4.2 Inhibitory Feedback Only. We now consider the opposite limiting case of purely inhibitory feedback. The equation of interest is 4.8, with $\beta_e = 0$, that is,

$$\frac{dg_i}{dt} = \beta_i f(0, g_i(t - \tau)) - g_i(t). \tag{4.14}$$

Fixed points of equation 4.14 satisfy

$$g_i = \beta_i f(0, g_i), \tag{4.15}$$

and since $f(0, g_i)$ is a nonincreasing function of g_i, we see that inhibitory feedback cannot produce multistability; that is, for each I, there is only one fixed point of equation 4.14. A similar result for a sigmoidal function f was shown in an der Heiden (1980). It is straightforward to show that nonzero solutions of equation 4.15 are possible only for $I_c < I$.

4.2.1 Stability. The linearization of equation 4.14 about a fixed point $\hat{g}$ is

$$\frac{dx}{dt} = \beta_i d_2 x(t - \tau) - x(t), \tag{4.16}$$

where d_2 is the derivative of f with respect to its second argument, evaluated at the fixed point $(g_e, g_i) = (0, \hat{g})$. Note that d_2 is nonpositive. Defining $A = \beta_i d_2$ and substituting $x = Be^{\lambda t}$ into equation 4.16, in a similar way to that done in section 4.1.1, we see that λ satisfies equation 4.12, with the newly defined A.

Assuming that we are above firing threshold, that is, $I_c < I$, we see that $A < 0$. Thus, for this parameter range, there are no bifurcations at which the eigenvalue $\lambda = 0$. As I is decreased toward I_c, A tends to $-\infty$. We prove below that as A does this, there is an infinite number of distinct values

of A at which pairs of roots of the characteristic equation 4.16 cross the imaginary axis and acquire a positive real part. The crossing of the first such pair brings on a Hopf bifurcation; the subsequent crossing of the other pairs alters the shape of the oscillation of the firing frequency: the closer the real parts of the root pairs are, the more the oscillation resembles a square wave. Similar behavior is seen in singularly perturbed delay-differential equations (see, e.g., Mensour & Longtin, 1998). Accordingly, such solutions can be qualified as bursting, since spikes occur in clusters separated by periods of quiescence. It is important to realize that such bursting solutions are due to the network, that is, to the feedback loop, since the core integrate-and-fire neuron with reversal potentials cannot burst autonomously. If, for large enough I, $-1 < A < 0$, the fixed point of equation 4.15 will be stable, and as I is decreased, it will lose stability through the first of the Hopf bifurcations.

To study Hopf bifurcations in equation 4.14, we substitute $\lambda = i\omega$ into equation 4.12, separate real and imaginary parts, and obtain the two equations

$$A\cos(\omega\tau) = 1 \tag{4.17}$$

and

$$A\sin(\omega\tau) = -\omega. \tag{4.18}$$

Note that for equation 4.17 to be satisfied, we require $1 \le |A|$.

From equations 4.17 and 4.18, we have that

$$\tau = \frac{\cos^{-1}(1/A) + 2n\pi}{\sqrt{A^2 - 1}} \tag{4.19}$$

at a Hopf bifurcation for some nonnegative integer n, and the frequency of oscillation (at the bifurcation) is given by $\omega = \sqrt{A^2 - 1}$. We claim that for a fixed $0 < \tau$ and any $n \in \{0, 1, 2, \ldots\}$, there is an $A \in (-\infty, -1)$ such that equation 4.19 is satisfied. To see this, note that equations 4.17 and 4.18 imply that $\cos^{-1}(1/A) \in (\pi/2, \pi)$. Thus, for any $n \in \{0, 1, 2, \ldots\}$, the function $\cos^{-1}(1/A) + 2n\pi$ is a monotonically increasing function of A, bounded below by $2n\pi + \pi/2$ and bounded above by $2n\pi + \pi$, for $A \in (-\infty, -1)$. The function $h(A) \equiv 1/\sqrt{A^2 - 1}$ is positive and monotonically increasing in the same interval, with $\lim_{A\to-\infty} h(A) = 0$ and $\lim_{A\to-1^-} h(A) = \infty$. Thus the range of the function on the right-hand side of equation 4.19 is $(0, \infty)$ for $A \in (-\infty, -1)$, and we have proved our claim.

It follows that for a fixed $0 < \tau$, there is an infinite number of distinct values of A, indexed by the integer n, satisfying equation 4.19, and thus an infinite number of values of I, accumulating from above at I_c, at which there is a Hopf bifurcation. Note that the most positive value of A at which

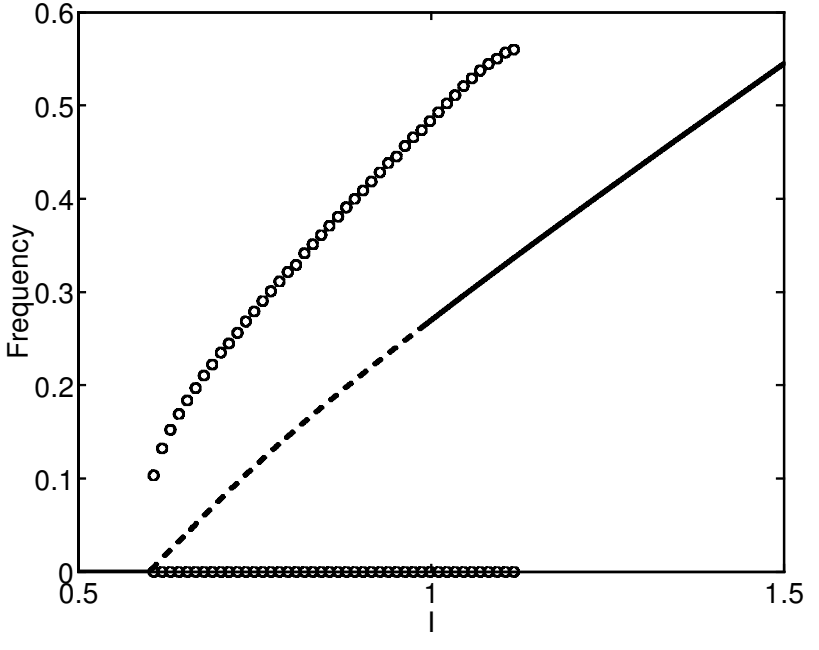

Figure 3: Dynamics of inhibitory delayed feedback. Frequency as a function of I for equation 4.14 with $\beta_e = 0$ and $\beta_i = 1$. Dashed line: unstable fixed point; solid line: stable fixed point; open circles: maximum and minimum frequency over one oscillation of g_i (stable). There is a subcritical Hopf bifurcation at $I \approx 0.98$. Other parameters are given in Table 1, and $\tau_i = 1$.

equation 4.19 is satisfied occurs for $n = 0$, and it is at this value that the fixed point loses its stability. This gives the condition 4.13.

In Figure 3, we show frequency as a function of I for $\beta_e = 0$ and $\beta_i = 1$. Simulations were performed using the software package `dde23` by Shampine and Thompson (2000). At the right, we see the branch of fixed points, which loses stability through a Hopf bifurcation as I is decreased. This is a subcritical bifurcation, and we conjecture that there is a branch of unstable periodic orbits emanating from this bifurcation and joining the branch of stable oscillations shown, in a saddle–node bifurcation of periodic orbits. We could not follow this conjectured branch of unstable periodic orbits with DDE–BIFTOOL, since this software is written under the assumption that the functions involved are differentiable everywhere, which is not the case for equation 3.1 (Engelborghs, Luzyanina, & Samaey, 2001).

The maximum frequency over one oscillation of the firing rate (open circles in Figure 3) appears to jump at $I = I_c = 0.6$. This is a result of using discrete values of I when calculating this quantity. Simulations suggest that

the maximum frequency during one oscillation tends to zero as I tends to I_c from above and that this curve has infinite slope at $I = I_c$. The actual frequency of oscillations in g_i also tends to zero as I tends to I_c from above, and simulations suggest that the period of oscillation scales as $-\log(I - I_c)$ as I tends to I_c from above (not shown). Both of these results are due to the nonsmoothness of the firing function f at $I = I_c$.

We note as well that the range of input current values over which the unstable fixed point occurs (the dashed line in Figure 3) can be made smaller by decreasing the inhibitory feedback strength β_i; the lower bound of this range is, however, always at $I_c = 0.6$. Thus, for smaller β_i, the oscillation should be seen only near the onset of firing; past the vicinity of this onset, one would see only constant firing rates, as for the usual leaky integrate-and-fire model in open loop. Interestingly, however, there will always be an oscillation not only for large β_i, but also no matter how small β_i is, or how small the minimal delay is; one can, in fact, always bring I closer to I_c to see the oscillation. This is due to the fact that the effective feedback gain is A, which involves not only β_i but also the value d_2 of the derivative of the firing function f with respect to its second argument. There will always be an I close enough to I_c (with $I > I_c$) such that d_2 is sufficiently negative (i.e., for a Hopf bifurcation to have occurred).

In Figure 4, we show the curves of Hopf bifurcations and conjectured saddle-node bifurcations of periodic orbits in the I, β_i plane. The conjectured curve was found by following a periodic orbit as I was increased until the system suddenly switched to a fixed point (see Figure 3). For parameter values between the two curves in Figure 4, the system 4.14 is bistable, with both a fixed value of g_i and periodic oscillations of it being stable.

4.3 Paired Feedback. To investigate the effects of paired feedback on the firing of the leaky integrate-and-fire neuron, we keep the total amount of feedback constant but move smoothly from purely excitatory feedback to purely inhibitory. We do this by introducing a parameter $\phi \in (0, 1)$ and writing

$$\beta_e = \phi\beta \quad \text{and} \quad \beta_i = (1 - \phi)\beta, \tag{4.20}$$

where, loosely speaking, β is the total feedback gain. Substituting this into equation 4.8, we obtain

$$\frac{dg_i(t)}{dt} = (1 - \phi)\beta f(\phi g_i(t - \tau)/(1 - \phi), g_i(t - \tau)) - g_i(t) \tag{4.21}$$

for $\phi \neq 1$. The extreme cases, $\phi = 0$ and $\phi = 1$, have been discussed above. In Figure 5, we show the situation for $\beta = 1$. We see that the bifurcation curves meet at the point $(I, \phi) = (0.6, 0.8667)$. For this value of ϕ, ϕ_c, the two types of feedback are balanced in the sense that there is neither the bistability

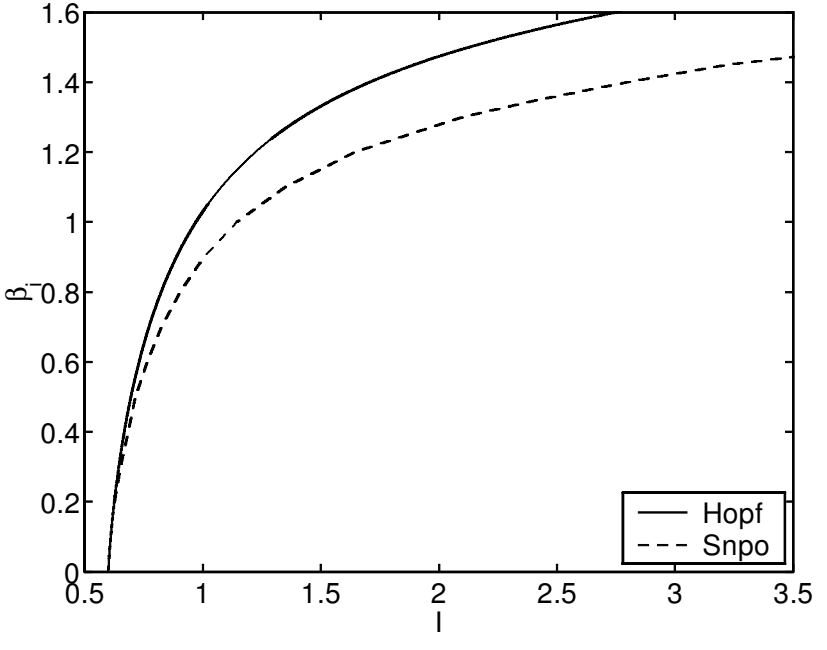

Figure 4: The curve of Hopf bifurcations (solid line) and conjectured saddle–node bifurcations of periodic orbits (dashed line) for equation 4.14 with $\beta_e = 0$ (inhibitory feedback only). Other parameters are given in Table 1. There is bistability between the two curves.

induced by excitatory feedback nor the oscillations induced by inhibitory feedback. This particular value of ϕ_c is determined by the threshold and reversal potentials and is the solution of

$$\frac{\phi_c V_e}{1-\phi_c} + V_i = \frac{V_\theta}{1-\phi_c}. \tag{4.22}$$

Recalling that the attractor of equations 4.2 and 4.3 lies on the line $g_e = \beta_e g_i/\beta_i = \phi g_i/(1-\phi)$, it can be shown that if equation 4.22 holds and $I = I_c = g_L(V_\theta - V_L)$, then V_{ss} is equal to V_θ for all g_i and a plot of

$$(1-\phi_c)\beta f(\phi_c g_i/(1-\phi_c), g_i) \tag{4.23}$$

as a function of g_i is just the zero function. Perturbing ϕ from ϕ_c breaks this degeneracy, and by plotting equation 4.23 as a function of g_i in a neighborhood of $(I, \phi) = (I_c, \phi_c)$, we see that only for $\phi_c < \phi$ and $I < I_c$ do we obtain multiple steady states of equation 4.21.

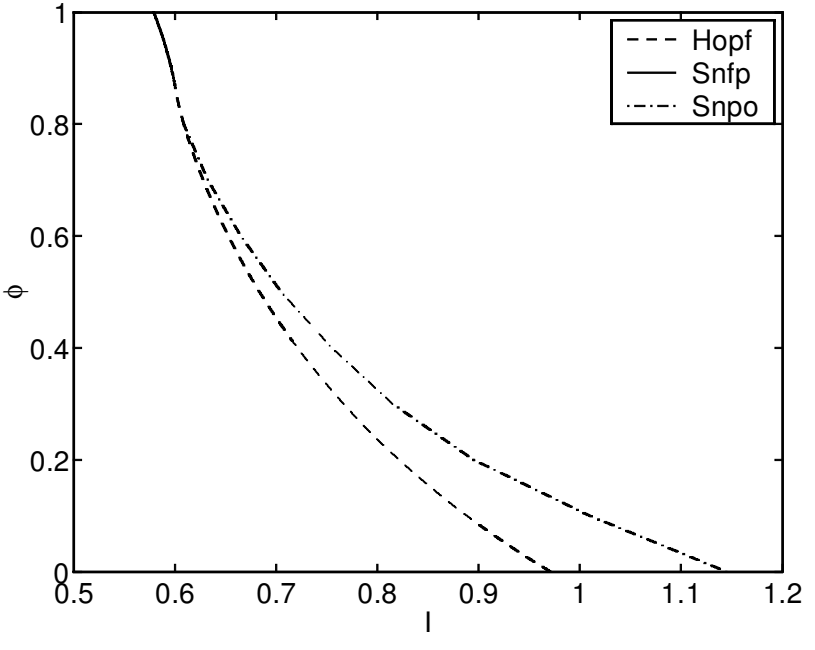

Figure 5: Curves of Hopf bifurcations (dashed line), conjectured saddle–node bifurcations of periodic orbits (dash–dotted line), and saddle–node bifurcations of fixed points (solid line) for (4.8) with $\beta = 1$ and the parametrization (4.20). Other parameters are given in Table 1. Two other bifurcation curves are not shown; see the text. The line $\phi = 0$ corresponds to Figure 3 (inhibition only), and the line $\phi = 1$ corresponds to a slice at $\beta_e = 1$ in Figure 2 (excitation only).

Note that in Figure 5, there are two other bifurcation curves not shown: one is the line $(I, \phi) \in 0.6 \times [0.8667, 1]$, along which the stable fixed point at the origin and the unstable fixed point on the middle branch are destroyed (see Figure 1). The other is the line $(I, \phi) \in 0.6 \times [0, 0.8667]$, along which the branch of oscillatory solutions created in the Hopf bifurcation are destroyed.

4.3.1 Chaotic Solutions. For strong enough feedback it is possible that equation 4.21 can have chaotic solutions. Motivated by the results of Mackey and Glass (1977), we choose parameters so that

$$(1 - \phi)\beta f(\phi g/(1 - \phi), g) \tag{4.24}$$

is a unimodal function of g, for example, $\beta = 7$ and $\phi = 0.85$ (see Figure 6). By choosing an appropriate delay (in this case, $\tau = 8$), chaotic solutions of equation 4.21 are observed (see Figure 7).

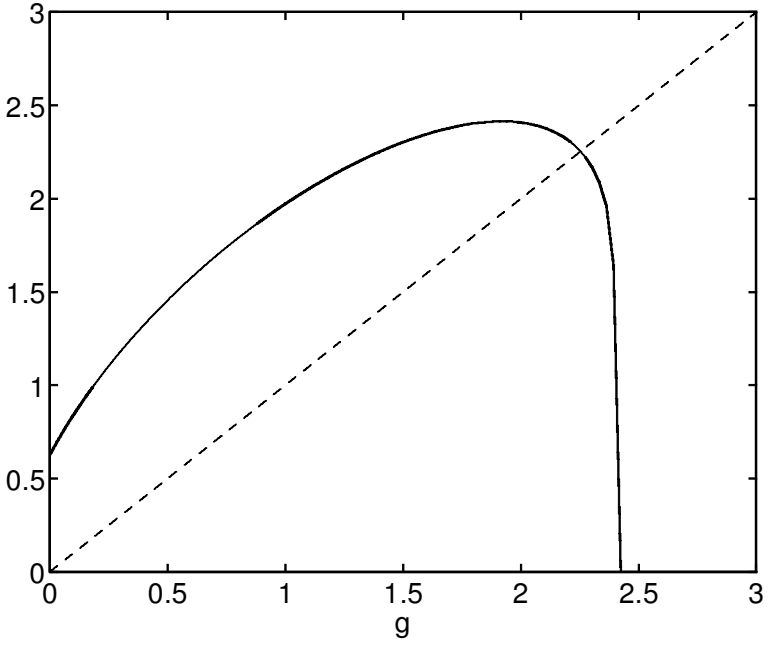

Figure 6: The function 4.24 for $\beta = 7$, $\phi = 0.85$ and $I = 1$. The dashed line is the diagonal. Other parameters are given in Table 1.

5 Gamma-Type Kernels with $m = 1$

We now move on to the case when $m = 1$. The delay kernel 2.7 now rises smoothly from zero at τ_e to its maximum at time $\tau_e + 1/a$, before decaying back to zero. A similar statement applies for $G_i^{m_i}$. We still assume that $a_e = a_i = 1$, and $\tau_e = \tau_i = \tau$. The governing equations are

$$\frac{dg_e}{dt} = \beta_e y_0 - g_e \tag{5.1}$$

$$\frac{dy_0}{dt} = f(g_e(t-\tau), g_i(t-\tau)) - y_0 \tag{5.2}$$

$$\frac{dg_i}{dt} = \beta_i z_0 - g_i \tag{5.3}$$

$$\frac{dz_0}{dt} = f(g_e(t-\tau), g_i(t-\tau)) - z_0 \tag{5.4}$$

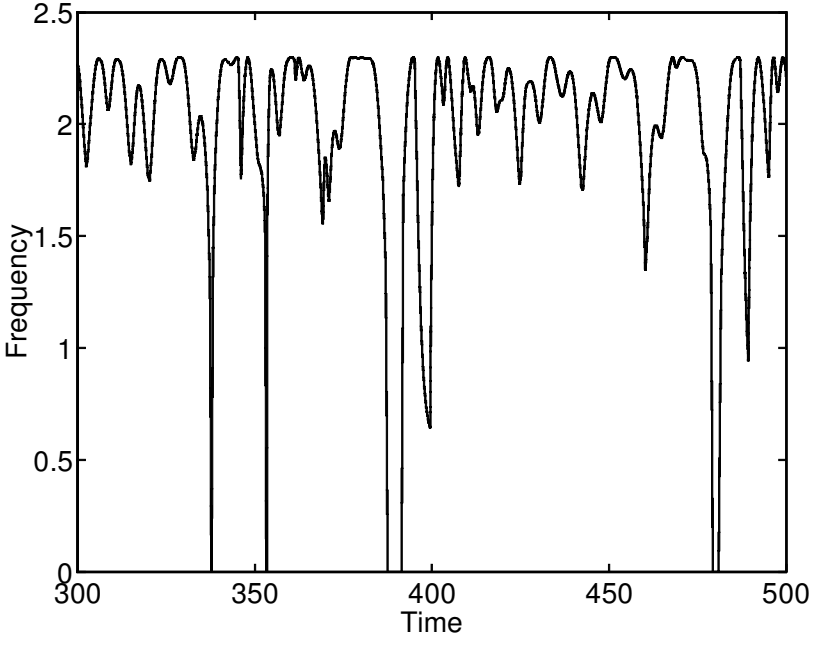

Figure 7: A chaotic solution of equation 4.21 for $I = 1$, $\beta = 7$, $\phi = 0.85$, $\tau = 8$. Note that the frequency is zero during some time intervals. Other parameters are given in Table 1.

where, if not specified, the functions on the right-hand sides are evaluated at time t. Similar to the case $m = 0$, we have a theorem regarding the existence of an attracting invariant manifold.

Theorem 1. *If both β_i and β_e are nonzero, then the attractor of equations 5.1 through 5.4 lies on the attracting invariant manifold on which $y_0 = z_0$ and $g_e = \beta_e g_i/\beta_i$. Thus, the dynamics on the attractor are governed by the system*

$$\frac{dg_i}{dt} = \beta_i z_0 - g_i \tag{5.5}$$

$$\frac{dz_0}{dt} = f(\beta_e g_i(t-\tau)/\beta_i, g_i(t-\tau)) - z_0. \tag{5.6}$$

Proof. Define s to be $s \equiv (y_0 - z_0)^2 + (2/\beta_e^2)(g_e - \beta_e g_i/\beta_i)^2$. Note that s is zero only on the manifold mentioned above. Now

$$\frac{ds}{dt} = -2[(y_0 - z_0)^2 + (2/\beta_e)(g_e - \beta_e g_i/\beta_i)(z_0 - y_0) + (2/\beta_e^2)(g_e - \beta_e g_i/\beta_i)^2]. \tag{5.7}$$

Now the right-hand side (r.h.s.) of equation 5.7 is negative except when s is zero, and thus trajectories approach the manifold on which $s = 0$. By considering the time evolution of $(z_0 - y_0)$ and of $(g_e - \beta_e g_i/\beta_i)$ from equation 5.1 through 5.4, it is clear that the manifold is invariant.

Note that if either β_e or β_i is zero, we only need consider half of the variables.

The linearization of equations 5.5 and 5.6 about a fixed point is

$$\frac{dx_1}{dt} = \beta_i x_2 - x_1 \tag{5.8}$$

$$\frac{dx_2}{dt} = [\beta_e d_1/\beta_i + d_2]x_1(t-\tau) - x_2, \tag{5.9}$$

where $d_{1/2}$ is the derivative of f with respect to its first/second argument, evaluated at the fixed point. Looking for solutions of the form $[x_1\ x_2]^T = Be^{\lambda t}$, where $B \in \mathbf{R}^2$ and x^T denotes the transpose of x, we find that λ satisfies

$$\lambda^2 + 2\lambda + 1 - (\beta_e d_1 + \beta_i d_2)e^{-\lambda\tau} = 0. \tag{5.10}$$

Note that this equation is still valid even if $\beta_i = 0$, as an analysis of equations 5.1 through 5.4 shows. Equations such as 5.10 arise in the analysis of linear oscillators with delayed feedback (Campbell, 1999; Stepán 1989).

Defining $A \equiv \beta_e d_1 + \beta_i d_2$, we have a theorem regarding the roots of equation 5.10:

Theorem 2. *If either $-1 < A < 1$, or $A < -1$ and*

$$\tau < \frac{\cos^{-1}[(2+A)/A]}{\sqrt{-A-1}}, \tag{5.11}$$

then all roots of equation 5.10 have negative real part.

Proof. When $A = 0$, the only roots of equation 5.10 are $\lambda = -1$, so the corresponding fixed point of equations 5.5 and 5.6 is stable. The only way the fixed point can become unstable is by λ crossing the imaginary axis. Substituting $\lambda = i\omega$ into equation 5.10, where ω is real, we have the equations

$$A\cos(\omega\tau) = 1 - \omega^2 \tag{5.12}$$

$$A\sin(\omega\tau) = -2\omega. \tag{5.13}$$

By squaring equations 5.12 and 5.13 and then adding them together, we obtain

$$A^2 = (1+\omega^2)^2. \tag{5.14}$$

First, consider increasing A. Equation 5.14 cannot be satisfied (i.e., we cannot have a Hopf bifurcation) for $0 \leq A < 1$, and the first bifurcation to occur as A is increased from 0 is at $A = 1$, when $\lambda = 0$. Thus, the fixed point is stable for $0 \leq A < 1$.

Now decrease A from 0. From equation 5.10, we see that a bifurcation at $\lambda = 0$ cannot occur. If a Hopf bifurcation occurs, the value of ω at the bifurcation is given by $\omega = \sqrt{-A-1}$. Note that since ω is real, we must have $A < -1$ for such a bifurcation to occur. Substituting this expression for ω into equation 5.12, we obtain

$$\tau = \frac{\cos^{-1}[(2+A)/A] + 2n\pi}{\sqrt{-A-1}} \tag{5.15}$$

for $n \in \{0, 1, 2, \ldots\}$, and by plotting the expression on the right-hand side of equation 5.15 as a function of A for different n (recalling that $A < -1$), we see that the fixed point will lose stability when the inequality 5.11 is violated, corresponding to the case $n = 0$.

Essentially the same theorem was presented by Campbell (1999), although care must be taken regarding the sign of A when comparing those results with the one presented here.

5.1 Excitation Only. We now consider the case when $\beta_i = 0$. The equations are

$$\frac{dg_e}{dt} = \beta_e y_0 - g_e \tag{5.16}$$

$$\frac{dy_0}{dt} = f(g_e(t-\tau), 0) - y_0. \tag{5.17}$$

Note that fixed points satisfy $g_e = \beta_e f(g_e, 0)$, which is the same as the condition for $m = 0$, equation 4.10. This is in fact the case for arbitrary m, which is not surprising, since changing m changes only the time course of the convolution kernel, equation 2.7. (It also changes the number of ODEs in equations 2.19 through 2.22, but these do not affect the values of the fixed points.)

Thus, the fixed points of equations 5.16 and 5.17 are as described in section 4.1, and the stability arguments for the three possible branches of solutions presented there also carry through. When they exist, the upper and zero branches are stable, and the middle branch is unstable.

5.2 Inhibition Only. With $\beta_e = 0$, the governing equations are

$$\frac{dg_i}{dt} = \beta_i z_0 - g_i \tag{5.18}$$

$$\frac{dz_0}{dt} = f(0, g_i(t-\tau)) - z_0. \tag{5.19}$$

As argued in section 5.1, the fixed points are the same as for the $m = 0$ case; for each value of I, there is only one fixed point. Also, $A < 0$ if we are above the firing threshold, and so there cannot be any bifurcations at which $\lambda = 0$. If $A < -1$, it is possible to have a Hopf bifurcation. In fact, there is an infinite number of Hopf bifurcations as I decreases, just as there was for $m = 0$, although the conditions for bifurcation are not the same.

Recall that at a Hopf bifurcation,

$$\tau = \frac{\cos^{-1}[(2+A)/A] + 2n\pi}{\sqrt{-A-1}} \tag{5.20}$$

for some nonnegative integer n. Following a similar argument to that in section 4.2.1, we observe that $\cos^{-1}[(2+A)/A] + 2n\pi$ is a monotonically increasing function of A, bounded below by $2n\pi$ and above by $(2n+1)\pi$ for $A \in (-\infty, -1)$, and that $h(A) \equiv 1/\sqrt{-A-1}$ is positive and monotonically increasing on the same interval, with $\lim_{A\to-\infty} h(A) = 0$ and $\lim_{A\to-1} h(A) = \infty$. We can see that for a fixed $\tau > 0$ and $n \in \{0, 1, 2, \ldots\}$, there is an $A \in (-\infty, -1)$ satisfying equation 5.20. Thus, there are an infinite number of values of I at which Hopf bifurcations occur, accumulating from above on the threshold for firing.

Note that the most positive value of A for which equation 5.20 is satisfied occurs when $n = 0$, as was the case in section 4.2.1 for $m = 0$. Also,

$$\frac{\cos^{-1}(1/A)}{\sqrt{A^2-1}} < \frac{\cos^{-1}[(2+A)/A]}{\sqrt{-A-1}} \tag{5.21}$$

for $A \in (-\infty, -1)$, so the first Hopf bifurcation that occurs as I is decreased occurs at a smaller value of I in the case $m = 1$, as compared with the case $m = 0$.

A plot of frequency as a function of I for equations 5.18 and 5.19 is qualitatively the same as Figure 3, except that the Hopf bifurcation and apparent saddle–node bifurcation of periodic orbits occur for I values slightly smaller than those in Figure 3.

5.3 Paired Feedback. If we parameterize β_e and β_i as in equation 4.20, we obtain a picture qualitatively similar to Figure 5, the only difference being that the curves of Hopf bifurcations and presumed saddle–node bifurcations of periodic orbits lie slightly to the left of those shown in Figure 5 (not shown).

6 General m

We now consider the case of general $m = m_e = m_i$, keeping $a_e = a_i = 1$ and $\tau_e = \tau_i = \tau$. Increasing the value of m while keeping the mean delay

fixed amounts to a sharper localization in time of the delayed feedback. The case $m \to \infty$ corresponds to a delta function delay kernel. As in the cases $m = 0, 1$, we have a theorem regarding the existence of an attracting invariant manifold:

Theorem 3. *If $1 < m$ and neither β_e nor β_i are zero, then there is an attracting invariant manifold on which*

$$[g_e, y_{m-1}, \ldots, y_0, g_i, z_{m-1}, \ldots, z_0] = [\beta_e g_i/\beta_i, z_{m-1}, \ldots, z_0, g_i, z_{m-1}, \ldots, z_0] \tag{6.1}$$

that is, the excitatory dynamics are slaved to the inhibitory ones (assuming that $\beta_i \neq 0$).

Proof. Similarly to theorem 1, define

$$s \equiv (1/\beta_e^2)(g_e - \beta_e g_i/\beta_i)^2 + \sum_{i=0}^{m-1}(y_i - z_i)^2.$$

We have

$$\frac{ds}{dt} = (2/\beta_e^2)(g_e - \beta_e g_i/\beta_i)[\beta_e(y_{m-1} - z_{m-1}) - (g_e - \beta_e g_i/\beta_i)] \tag{6.2}$$

$$-2\sum_{i=0}^{m-1}(y_i - z_i)^2 + 2\sum_{i=1}^{m-1}(y_i - z_i)(y_{i-1} - z_{i-1}), \tag{6.3}$$

which can be rewritten as

$$\frac{ds}{dt} = -(2/\beta_e^2)(g_e - \beta_e g_i/\beta_i)^2 + (2/\beta_e)(y_{m-1} - z_{m-1})(g_e - \beta_e g_i/\beta_i) - (y_{m-1} - z_{m-1})^2 \tag{6.4}$$

$$-\sum_{i=2}^{m-1}[(y_i - z_i)^2 - 2(y_i - z_i)(y_{i-1} - z_{i-1}) + (y_{i-1} - z_{i-1})^2] \tag{6.5}$$

$$-[(y_1 - z_1)^2 - 2(y_1 - z_1)(y_0 - z_0) + 2(y_0 - z_0)^2]. \tag{6.6}$$

Since $0 < \beta_e$, the right-hand side of equation 6.4 is negative when $s \neq 0$ and zero otherwise. All terms within the square brackets in equation 6.5 are either positive or zero, and the term within the square brackets in equation 6.6 is positive when $s \neq 0$ and zero otherwise. Hence, $ds/dt < 0$ except when $s = 0$, when $ds/dt = 0$. Thus, trajectories approach the manifold on which $s = 0$. Proceeding further by substitution as in the proof of theorem 5.1, we see that the manifold is invariant. (Note that if either β_i or β_e are zero, we still need consider only half of the variables.)

The excitatory dynamics are slaved to the inhibitory ones, whose dynamics are given by

$$\frac{dg_i}{dt} = \beta_i z_{m-1} - g_i \tag{6.7}$$

$$\frac{dz_{m-1}}{dt} = z_{m-2} - z_{m-1} \tag{6.8}$$

$$\vdots \tag{6.9}$$

$$\frac{dz_1}{dt} = z_0 - z_1 \tag{6.10}$$

$$\frac{dz_0}{dt} = f(\beta_e g_i(t-\tau)/\beta_i, g_i(t-\tau)) - z_0, \tag{6.11}$$

where, if an argument is not given, the quantity is evaluated at time t. Performing the usual stability analysis, we find that if λ is an eigenvalue associated with the linearization of equations 6.7 through 6.11 about a fixed point, the determinant of the following matrix must be zero:

$$B \equiv \begin{pmatrix} \lambda+1 & -\beta_i & 0 & \cdots & \cdots & 0 \\ 0 & \lambda+1 & -1 & 0 & \cdots & 0 \\ \vdots & & \vdots & & & \vdots \\ 0 & \cdots & \cdots & 0 & \lambda+1 & -1 \\ -\widehat{A}e^{-\lambda\tau} & 0 & \cdots & \cdots & 0 & \lambda+1 \end{pmatrix},$$

where $\widehat{A} \equiv \beta_e d_1/\beta_i + d_2$. It is straightforward to show that $\det B = 0$ is equivalent to

$$(\lambda+1)^{m+1} = Ae^{-\lambda\tau}, \tag{6.12}$$

where $A \equiv \beta_e d_1 + \beta_i d_2$, as in section 5. We have a zero eigenvalue when $A = 1$. Setting $\lambda = i\omega$ in equation 6.12 and taking magnitudes, where ω is real, we have

$$(1+\omega^2)^{m+1} = A^2. \tag{6.13}$$

We have the following theorem:

Theorem 4. *The roots of equation 6.12 have negative real part for* $0 \le A < 1$.

Proof. We know that for $A = 0$, the roots of equation 6.12 are $\lambda = -1$. If a pair of roots pass through the imaginary axis with nonzero imaginary part, condition 6.13 must hold. This cannot be satisfied for $0 < A < 1$. A real root can pass through the imaginary axis at $A = 1$, and by differentiating equation 6.12 with respect to A, we see that this eigenvalue passes transversely through the imaginary axis.

Table 2: Bifurcation Conditions on τ and A.

m	ω^2	τ
0	A^2-1	$f_0^n(A) \equiv \{\cos^{-1}(1/A)+2n\pi\}/\sqrt{A^2-1}$
1	$-A-1$	$f_1^n(A) \equiv \{\cos^{-1}[(2+A)/A]+2n\pi\}/\sqrt{-A-1}$
2	$\sqrt[3]{A^2}-1$	$f_2^n(A) \equiv \{\cos^{-1}[(4-3\sqrt[3]{A^2})/A]+2n\pi\}/\sqrt{\sqrt[3]{A^2}-1}$
3	$\sqrt{-A}-1$	$f_3^n(A) \equiv \{\cos^{-1}[(8-8\sqrt{-A}-A)/A]+2n\pi\}/\sqrt{\sqrt{-A}-1}$

We can see that the only way the fixed point can lose stability as A is decreased from 0 is through a Hopf bifurcation, and that this can occur only for $A < -1$. Setting $\lambda = i\omega$ in equation 6.12 and separating the real and imaginary parts, we obtain the conditions in Table 2 for τ as a function of A at such bifurcations. We have included the cases $m = 0, 1$ for comparison, and also tabulate ω^2, where $n \in \{0, 1, 2 \ldots\}$. Entries for $m > 3$ are straightforward but tedious to derive. In Figure 8, we plot f_2^n and f_3^n for $n = 0, 1$ and 2. Interestingly, f_2^0 has a vertical asymptote at $A = -8$, and f_3^0 has a vertical asymptote at $A = -4$. (It can be shown that these curves are not defined to the left of their asymptotes, since we require both τ and ω to be positive.)

Because of the nesting of the curves and our previous results for $m = 0, 1$, we see that the fixed point of equations 6.7 through 6.11 will lose stability as A decreases through the curve $\tau = f_m^0(A)$ for $m = 0, 1, 2$ and 3. Combined with theorem 4, this gives the following conditions for stability of the fixed point of equations 6.7 through 6.11:

Theorem 5.

- *For the case $m = 2$. If either $-1 < A < 1$, or $-8 < A < -1$ and $0 < \tau < f_2^0(A)$, all roots of equation 6.12 have negative real part.*
- *For the case $m = 3$. If either $-1 < A < 1$, or $-4 < A < -1$ and $0 < \tau < f_3^0(A)$, all roots of equation 6.12 have negative real part.*

The proof can be constructed from the statements above, and is similar to that presented in Campbell (1999).

Because of the vertical asymptote of f_2^0 at $A = -8$, the Hopf bifurcation at which the fixed point loses stability must occur for $-8 < A$, no matter how small τ is. This is in contrast with the cases $m = 0, 1$, where by decreasing τ, the value of A at which the first Hopf bifurcation occurred could be made arbitrarily large and negative. Similarly, for $m = 3$, the Hopf bifurcation at which the fixed point loses stability must occur for $-4 < A$.

7 Breaking Symmetries

In this section we investigate the effects of breaking the various symmetries $\tau_i = \tau_e$, $a_i = a_e$, and $m_i = m_e$.

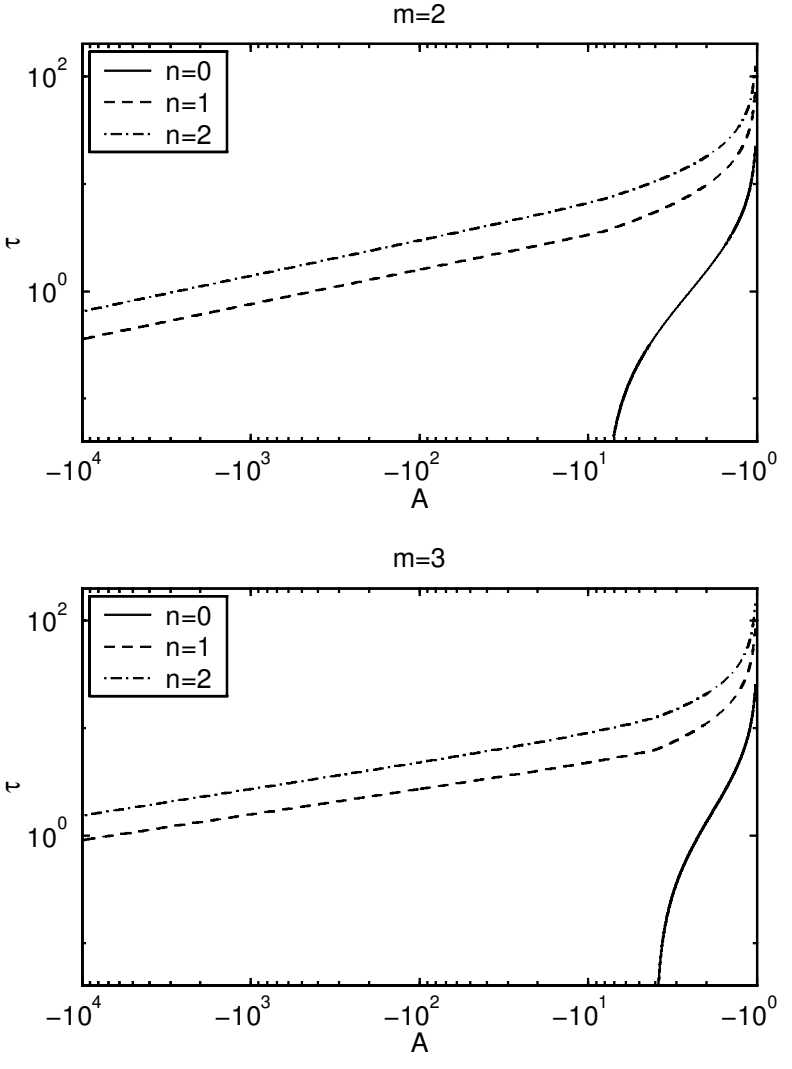

Figure 8: Relation between τ and $A = \beta_e d_1 + \beta_i d_2$ (defined after theorem 1) at selected crossings of pairs of eigenvalues into the right-hand complex plane (the crossing conditions being defined in Table 2). (Top) f_2^0 (solid line), f_2^1 (dashed line), and f_2^2 (dash-dotted line). Bottom: f_3^0 (solid line), f_3^1 (dashed line) and f_3^2 (dash-dotted line). The functions are defined in Table 2. Note that f_2^0 has a vertical asymptote at $A = -8$, and f_3^0 has a vertical asymptote at $A = -4$. Note the logarithmic scales. The oscillations in firing rate appear increasingly singular (i.e., "bursty") as the boundaries for larger values of n are crossed.

7.1 Different Delays. We first break the symmetry of $\tau_e = \tau_i$, but keep $a_e = a_i = 1$. Thus, the convolution kernels 2.7 and 2.8 are no longer equal, and we can no longer slave the excitatory dynamics to the inhibitory. We consider the case $m = 0$. The extremes of $\beta_i = 0$ and $\beta_e = 0$ will be qualitatively the same as for the situation in which $\tau_e = \tau_i$, for the following reason:

- $\beta_i = 0$. The determination of the stability or instability of the fixed points depended on only A, not τ_e. This case is therefore identical to the case presented in section 4.1.
- $\beta_e = 0$. As in section 4.2, the only way a fixed point can be destabilized is through a Hopf bifurcation. These will occur when equation 4.19 is satisfied, where $\tau = \tau_i$. The stability arguments in section 4.2 hold for any $0 < \tau$, so the only effect of changing τ_i will be to change the exact values of A that satisfy equation 4.19.

However, the situation for paired feedback is different. The degenerate point at $(I, \phi) = (0.6, 0.8667)$ in Figure 5 breaks up into a set of codimension 2 points at which curves of codimension 1 bifurcations (e.g., Hopf bifurcations and saddle-node bifurcations) meet. We will not go into this breakup in detail here, but rather show a representative example of the effects of making $\tau_e \neq \tau_i$. We make the choice $\tau_i = 1$, $\tau_e = 3$, so the delay for the inhibitory feedback is smaller than for the excitatory. We keep $a_i = a_e = 1$. The equations are

$$\frac{dg_e}{dt} = \beta_e f(g_e(t - \tau_e), g_i(t - \tau_e)) - g_e(t) \tag{7.1}$$

$$\frac{dg_i}{dt} = \beta_i f(g_e(t - \tau_i), g_i(t - \tau_i)) - g_i(t). \tag{7.2}$$

We parameterize β_e and β_i as in equation 4.20. A plot of frequency as a function of I for $\beta = 1$, $\phi = 0.9$ is shown in Figure 9. There are several interesting aspects to this figure. First, there are oscillations in frequency for $I < I_c = 0.6$ and for $0.8667 < \phi$ (contrast with Figure 5). Second, neither of the fixed points created in the saddle-node bifurcation is stable in a neighborhood of the bifurcation (contrast with Figure 1). Third, the system is tristable for $0.5976 < I < 0.6$, as the zero solution (which exists for $I < 0.6$), the nonzero fixed point, and the periodic oscillation are all stable. Note that the range of I values over which there is tristability is relatively narrow; this could presumably be increased by varying other parameters. We conjecture that there is a branch of unstable periodic orbits emanating from the subcritical Hopf bifurcation and terminating at a saddle-node bifurcation of periodic orbits at $I = 0.6045$. We were unable to numerically confirm this (see below). The bifurcation terminating the oscillations as I is decreased has not been determined, as we could not follow the periodic

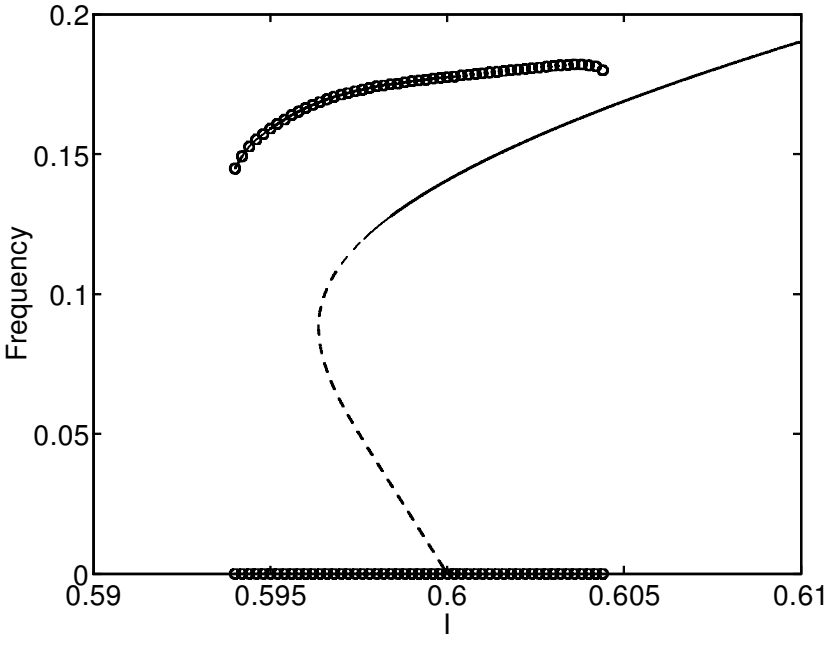

Figure 9: Breaking symmetries with differing delays, in the case where excitation dominates. Frequency as a function of I for equations 7.1 and 7.2 with $\beta_e = 0.9$, $\beta_i = 0.1$, $\tau_i = 1$, $\tau_e = 3$. Other parameters are as given in Table 1. Solid line: stable fixed point; dashed line: unstable fixed point; open circles: maximum and minimum frequency over one oscillation (stable). There is a subcritical Hopf bifurcation at $I \approx 0.5976$.

orbit with DDE-BIFTOOL due to the nondifferentiability of the firing-rate function.

7.2 Different Values of a. We now consider the case $a_i = 5$, $a_e = 1$, keeping $\tau_i = \tau_e = 1$, with $m = 0$. (Varying a changes the rate at which the convolution kernels 2.7 and 2.8 decay.) As argued in section 7.1, the case $\beta_i = 0$ is unchanged. For $\beta_e = 0$, we again lose stability of the fixed point via a Hopf bifurcation as I is decreased. If $a_i \neq 1$, equation 4.19 should be replaced by

$$\tau_i = \frac{\cos^{-1}(1/A) + 2n\pi}{a_i\sqrt{A^2 - 1}}. \tag{7.3}$$

Thus, changing a_i only changes the precise values of A at which equation 7.3 is satisfied, and we still have an infinite number of Hopf bifurcations as I is

decreased. Note that at such a Hopf bifurcation, the frequency of oscillation is $\omega = a_i\sqrt{A^2 - 1}$, so changing a_i will change the frequencies of oscillation.

In a similar way to that described in section 7.1, breaking the symmetry of $a_i = a_e$ breaks up the point $(I, \phi) = (0.6, 0.8667)$ in Figure 5 into a set of lower codimension points. For the case $a_i = 5$, $a_e = 1$, $\tau_i = \tau_e = 1$, $\beta = 1$, $\phi = 0.88$, a plot of frequency as a function of I is qualitatively the same as Figure 9 (not shown).

7.3 Different Values of m. We consider the case $m_i = 0$ and $m_e = 1$, keeping $\tau_e = \tau_i = \tau$ and $a_i = a_e = 1$. The system is then

$$\frac{dg_e}{dt} = \beta_e y_0 - g_e \tag{7.4}$$

$$\frac{dy_0}{dt} = f(g_e(t-\tau), g_i(t-\tau)) - y_0 \tag{7.5}$$

$$\frac{dg_i}{dt} = \beta_i f(g_e(t-\tau), g_i(t-\tau)) - g_i. \tag{7.6}$$

This has an attracting invariant manifold given by $g_i = \beta_i y_0$, on which the dynamics are given by

$$\frac{dg_e}{dt} = \beta_e y_0 - g_e \tag{7.7}$$

$$\frac{dy_0}{dt} = f(g_e(t-\tau), \beta_i y_0(t-\tau)) - y_0. \tag{7.8}$$

7.3.1 Inhibition Only. We have

$$\frac{dy_0}{dt} = f(0, \beta_i y_0(t-\tau)) - y_0. \tag{7.9}$$

Using $g_i = \beta_i y_0$, we see that this is equivalent to equation 4.14, and the analysis is exactly the same as described for the "inhibition only" case discussed in section 4.2.

7.3.2 Excitation Only. If $\beta_i = 0$, equations 7.7 and 7.8 are the same as equations 5.16 and 5.17, and their analysis is described in section 5.1.

7.3.3 Paired Feedback. The situation is very similar to that described in sections 7.1 and 7.2, with the breakup of the degenerate point into a number of lower codimension points. A plot of frequency as a function of I for $\phi = 0.87$ is qualitatively similar to Figure 9 (not shown).

Since breaking any of the symmetries discussed in this section causes the breakup of the point $(I, \phi) = (0.6, 0.8667)$ in Figure 5 into codimension 2

points (not shown), we do not expect that any further breaking of symmetries (e.g., simultaneously having $\tau_i \neq \tau_e$ and $a_i \neq a_e$) would introduce any more novel behavior; rather, it would just move these points around in the I, ϕ plane. These codimension 2 points could be analyzed in detail by linearizing the appropriate systems about fixed points and investigating their stability.

8 Stochastic Paired Delayed Feedback

The analysis until now has been in the deterministic case, where there is a well-defined threshold for periodic firing in equation 2.2. However, noise is ubiquitous in neural systems, mainly as a result of the probabilistic nature of synaptic transmission (Koch, 1999). It is well known that including stochastic effects in single-neuron models "smoothes out" the abrupt change in slope of the frequency versus input current relationship that is seen in type I neurons (Hohn & Burkitt, 2001; Lansky & Sacerdote, 2001), of which the integrate–and–fire neuron we have studied is an example. How does this smoothing change the dynamics of the neuron with paired delayed feedback described up to now? This is a very broad and difficult question, especially since there are a number of ways to include noise such as synaptic noise in neuron models, and there are very few results in the literature on noise-driven systems with memory. The main difficulty in analyzing such systems stems from the non-Markovian nature of the problem, which precludes the use of standard tools such as Fokker-Planck analysis and the (related) first passage time to threshold calculations (Guillouzic, L'Heureux, & Longtin, 2000).

In this section, we approach this problem in a simple way, in the hope that the results will capture the essential effects of noise and, in particular, its smoothing of the firing function. We investigate the effects of noise of the leaky integrate-and-fire neuron with delayed feedback under study up to now by adding a stochastic term, $\sigma\xi(t)$, to equation 2.1, where $\xi(t)$ is gaussian white noise with zero mean and variance 1. The parameter σ adjusts the noise intensity. The firing rate of the neuron 2.1 is now given by (Ricciardi, 1977; Wang, 1999)

$$f = \left(\tau_r + \sqrt{\pi}\widehat{\tau}\int_a^b \exp(x^2)[1 + \mathrm{erf}(x)]\,dx\right)^{-1}, \tag{8.1}$$

where

$$\widehat{\tau} \equiv C/g_{tot} \tag{8.2}$$

$$a \equiv \frac{C(V_r - V_{ss})}{\sigma\sqrt{\widehat{\tau}}} \tag{8.3}$$

$$b \equiv \frac{C(V_\theta - V_{ss})}{\sigma\sqrt{\widehat{\tau}}}, \tag{8.4}$$

and the error function is defined as $\mathrm{erf}(x) = \frac{2}{\sqrt{\pi}} \int_0^x \exp(-t^2)\, dt$. Using asymptotic expansions, this expression can be shown to reduce to equation 2.2 in the limit of vanishing noise $\sigma \to 0$. The idea here is to assume that there is background current noise in the neuron, possibly due to synaptic noise and ionic conductance fluctuations, and that the intensity of this noise is independent of the feedback. The noise intensity is rather set, for example, by the feedforward input to the neuron, embodied in the mean bias current I. It is known that for Poisson statistics (which synaptic inputs are often assumed to have), the variance of the synaptic conductance noise increases with the mean frequency of arrival of spikes at the synapse. Thus, one can expect that if the neuron increases its firing rate, its feedforward inputs and associated noise will remain constant, but its feedback current will increase in both mean and variance. This change in variance will be neglected here as a first approximation to this problem of stochastic paired delayed feedback, and the feedback will change in time as in our previous noiseless analysis. Also, in accord with the assumption that the main noise is from feedforward rather than feedback input, the noise is ascribed to the parameter I rather than to the feedback conductances $g_e(t)$ and $g_i(t)$. Note that this noise could have included synaptic conductance noise had we explicitly modeled the feedforward synaptic input to the cell with conductances and reversal potentials, but that is an unnecessary complication for a first analysis of this problem.

Note that in the spirit of our formalism based on the firing function and firing rates, rather than the spiking dynamics of the neuron, the noise can be included in what is effectively a deterministic way through equation 8.1 (see also Brunel, 1996; Wang, 1999). Equations 2.19 through 2.26 are still deterministic, with the noise intensity modifying the function f; no stochastic simulations are needed. The model we now analyze is thus, strictly speaking, a deterministic model meant to represent the stochastic situation. Accordingly, we will assume that the inputs to the firing function change on a sufficiently slow timescale compared to the membrane time constant, such that the parameters of this function are slaved to the slower dynamics of the feedback conductances. In particular, the increase in feedback activity affects g_{tot} and $V_{ss}(t)$ as before, with σ fixed. This means that although we have made simplifications, the effect on firing of feedback conductance fluctuations, and thus the membrane time constant fluctuations, are being taken into account.

The smoothing effect of noise can be seen by comparing equation 8.1 with 2.2 for the deterministic case. There are several effects of adding noise in this way that are not present in the deterministic case. One is that there is now an upper bound on the absolute value of the derivative of f with respect to any of the variables. This will have a significant effect on the number of Hopf bifurcations that occur as I is varied (if any). Another effect is that there is no longer a threshold for firing, as f is never zero (although it does get extremely small for some values of its parameters and variables).

8.1 Numerical Implementation. We briefly discuss the problem of numerically implementing the integral in equation 8.1. Due to round-off error, many software packages (e.g., Matlab, MAPLE) return $\mathrm{erf}(x) = 1$ for $x > 6$ and $\mathrm{erf}(x) = -1$ for $x < -6$. However, the complementary error function, $\mathrm{erfc}(x) \equiv 1 - \mathrm{erf}(x)$, can often be accurately evaluated for $0 \le x < 27$, where the upper bound is determined by underflow. Thus, for $0 \le x < 27$, we can accurately evaluate $\exp(x^2)[1 + \mathrm{erf}(x)]$ as $2\exp(x^2) - \exp(x^2)\mathrm{erfc}(x)$. Using the oddness of erf, we can see that $1 + \mathrm{erf}(x) = \mathrm{erfc}(-x)$, so for $-27 < x < 0$, we can accurately evaluate $\exp(x^2)[1 + \mathrm{erf}(x)]$ as $\exp(x^2)\mathrm{erfc}(-x)$. If a larger range of x values is needed, one alternative is to use high-precision software, such as MAPLE, to evaluate $\exp(x^2)[1 + \mathrm{erf}(x)]$ using the above expressions at a finite number of values of x. These can then be interpolated between by the software being used for simulations. In particular, if the interpolation is used to provide an approximation to $\exp(x^2)[1 + \mathrm{erf}(x)]$ at a number of evenly spaced values of x, the integral in equation 8.1 can be approximated by standard methods of quadrature (e.g., Simpson's rule).

We now investigate the effects of noise on the previously computed behaviors, first for either excitatory and inhibitory feedback alone and then in combination.

8.2 Excitation Only. In this section, we examine the effects of noise on the behavior seen in section 4.1: $m_e = m_i = 0$, $\tau_e = \tau_i = 1$, $a_e = a_i = 1$, and $\beta_i = 0$. The results are shown in Figure 10. We see that noise "smoothes out" the sharp bifurcation that occurs at $I = 0.6$ in the deterministic case (see Figure 1). This is because the firing frequency is now a smooth function of its parameters and arguments. Also, there is now an upper limit on the absolute value of the slope of f. This means that the quantity $A = \beta_e d_1$ can no longer be made arbitrarily large in magnitude, even for arbitrarily small β_e, as was possible in the deterministic case. The consequence is that for small β_e or large σ, the system may not be multistable, with instead only one fixed point for all values of I. If there are three coexisting fixed points, the larger and smaller frequency ones are stable, and the middle one is unstable, as for the deterministic case.

With reference to Figure 2, the effect of noise is to move the curve shown there, together with the line $I = 0.6$, away from the I-axis. The two curves meet at a cusp, and this cusp moves further from the I-axis as σ is increased (not shown). Thus, for a fixed value of σ, there is an interval of β_e values (with $\beta_e = 0$ being one end of the interval) for which the system is not bistable. The width of this interval increases as σ increases.

8.3 Inhibition Only. We now discuss the stochastic version of section 4.2. The stability arguments still hold, but in contrast with the deterministic case, there is now an upper bound on the magnitude of A. Therefore, there is no longer an infinite number of Hopf bifurcations as I is decreased. Recalling the definition of A ($A = \beta_i d_2$), we see that for nonzero σ and arbi-

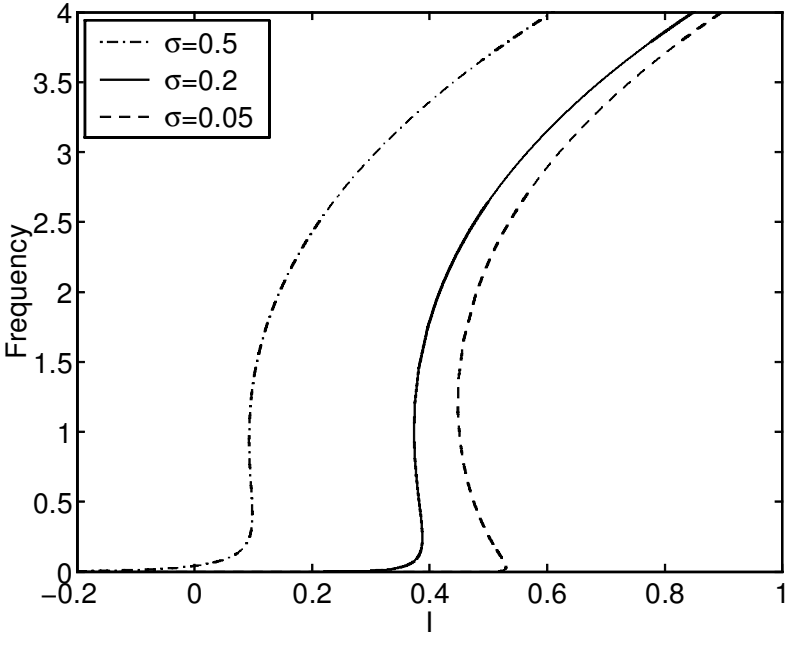

Figure 10: Frequency as a function of I for equation 4.9, where f is given by equation 8.1, for three different values of σ. $\beta_e = 2$. Compare with Figure 1. When three branches are present, the upper and lower ones are stable, and the middle branch is unstable. Other parameters are as given in Table 1.

trarily small β_i, there will not actually be any Hopf bifurcations, in contrast with the deterministic case.

In Figure 11, we show firing frequency as a function of I for two different values of σ, with $\beta_i = 1$. We see that the curve of fixed points is smoothed out and that increasing σ moves both the Hopf bifurcation at high I and the saddle–node bifurcation of periodic orbits to lower values of I. Increasing σ even further causes the right–most Hopf bifurcation to become supercritical rather than subcritical.

With reference to Figure 4, as σ is increased from zero, the two curves shown there, plus the curve lying on the line $I = 0.6$ on which oscillations are created, move away from the I-axis. The curve of Hopf bifurcations forms a U in the β_i, I plane, and the bottom of the U moves farther from the I-axis as σ is increased (not shown). Moving along the right branch of the U as β_i is increased, the Hopf bifurcation changes from supercritical to subcritical, so there is also a curve of saddle–node bifurcations of periodic orbits emanating from it.

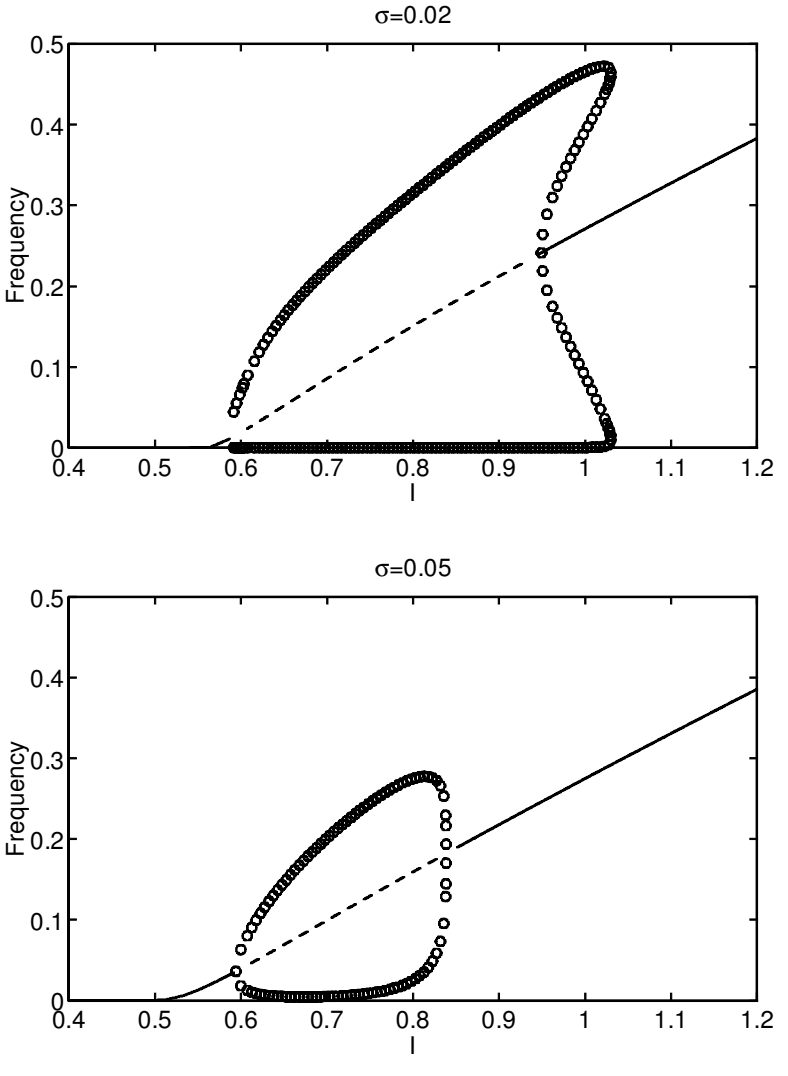

Figure 11: Frequency as a function of I for equation 4.14, where f is given by equation 8.1, for $\sigma = 0.02$ (top) and $\sigma = 0.05$ (bottom). Open circles indicate the maximum and minimum frequency over one period of oscillation. The dashed line indicates an unstable fixed point and the solid line a stable fixed point. In the top panel, the left Hopf bifurcation is supercritical and the right one is subcritical. In the bottom panel, both are supercritical. Compare with Figure 3. $\beta_i = 1$. Other parameters are as given in Table 1.

8.4 Paired Feedback. When noise is added to the system, the point at $(I, \phi) = (0.6, 0.8667)$ in figure 5 breaks up. For small noise intensity, the curve of Hopf bifurcations in that figure, together with the line $I = 0.6$ for $0 < \phi < 0.8667$, forms a $\cap$-shaped curve, emanating from the I-axis. The Hopf bifurcation on the right side of this curve may be subcritical over some of its extent, depending on the values of σ and β (not shown).

The curve of saddle–node bifurcations of fixed points in Figure 5, together with the line $I = 0.6$ for $0.8667 < \phi < 1$, form a cusp emanating from the line $\phi = 1$. Thus, when $\sigma \neq 0$, there is an interval of ϕ values (rather than just one value, as was the case for $\sigma = 0$) over which the feedback is "balanced," in the sense that it causes neither bistability not oscillations in frequency.

8.5 General Remarks. Adding noise does not destroy the chaotic behavior shown in section 4.3.1 (results not shown). This is to be expected, since the unimodal function shown in Figure 6 will not be destroyed by noise, merely smoothed out and shifted a little. In general, the effect of noise is to smooth out the discontinuity in the derivative of the firing function f and to put an upper bound on the absolute value of the derivative of this function. The effects of this on the existence and stability of fixed points then follow. Our analysis and numerics further reveal that there is generally a trade-off between feedback strength and noise intensity, in the following sense. As the noise intensity σ is increased, the feedback strength must also be increased to produce the qualitative features of the deterministic case.

9 Conclusion and Outlook

We have presented an investigation of the dynamics of a leaky integrate-and-fire neuron with paired (excitatory and inhibitory) delayed synaptic feedback. This neuron drives a population of postsynaptic cells, and these in turn project their activity back to the neuron via inhibitory and excitatory feedback, as seen, for example, in thalamocortical loops. The conductances modulated by this feedback were assumed to evolve on a slower timescale than the membrane time constant, a quasi-static approximation that is well justified, except perhaps for very fast synaptic input. This enabled us to replace the integrate-and-fire dynamics by the firing function associated with these dynamics under constant parameters. The conductances in the firing function were assumed to be weighted averages of the past firing rate. This integro-differential formulation was then converted to a coupled ordinary- and delay-differential equation formulation. The dimensionality of this system increased the narrower the delay distributions were. The model amounts to excitatory and inhibitory conductances modulating themselves and each other via the firing function in which the conductance parameters are assumed to be dynamical variables. Further, these conductances multiplied their corresponding "battery" terms involving reversal

potentials. Thus, the model properly treats the inherent time-dependent variations of the membrane time constant.

The model is also realistic in that it takes into account a possible minimal delay for the feedback, as well as the distribution of delays added to this minimal delay. This distribution characterizes the temporal spread of the feedback, that is, the distributed memory in the neural loop. The kernels for both feedback pathways can be used to model either direct feedback of the neuron onto itself or, alternately, feedback via one or more other neuron populations. Physiological data can then be used to fit the delay distributions and the feedback strengths (see, e.g., Mackey & an der Heiden, 1982; Berman & Maler, 1999; Eurich et al., 2002) and incorporate them into the model.

For excitatory feedback alone, our analysis revealed that the system can be quiescent, or fire periodically, or exhibit bistability between these two states. Inhibition alone produces quiescence, oscillatory firing rates, or bistability between constant and oscillatory firing-rate solutions. This means, for example, that an external input from, say, an afferent pathway can toggle the neural loop between periodic firing at a constant frequency and an oscillatory firing rate. Under certain conditions, this rate can reach low values, and the resulting pattern can look bursty, even though there is no intrinsic bursting mechanism in the integrate-and-fire neuron model by itself (i.e., in open loop). Thus, a neural loop involving inhibitory feedback (with or without excitatory feedback) can be switched between constant firing and network-dependent bursting. This is seen even if the excitatory feedback is much stronger than the inhibitory one (see Figure 9). This is certainly of interest for systems involving such loops and in which bursting is known to occur (see, e.g., Murphy et al., 1999; Berman & Maler, 1999).

Our analysis of the general paired feedback case has been made possible by the discovery of an invariant manifold for the dynamics. This case exhibits all the behaviors seen in the two limiting cases and allows for the possibility of deterministic chaos. Our analysis has shown how all the behaviors evolve as the balance between the two types of inhibition changes.

Our work has also investigated some of the effects on these bifurcations of the delay distribution width, as well as of possible mismatches between the delays or other parameters of the two pathways. In particular, our study defines the conditions under which the bistability and saturation effects associated with recurrent excitation can be modified by the stabilizing yet potentially oscillatory effects of inhibitory feedback.

Further, our analysis has compared the dynamical behaviors of this model in the deterministic case with a simple stochastic case. We investigated the effects of noise on such a system by modifying the function describing the firing rate of the neuron as a function of input in a well–established fashion (Ricciardi, 1977). This is a biophysically plausible way of studying the dynamics and bifurcations in recurrent nets with a smooth firing function—without having to add an ad hoc smoothing factor to the

deterministic firing function. We find here that the smoothing provided by the noise removes the degeneracy in the deterministic function at firing threshold, where the function is not differentiable. Adding noise puts an upper bound on the absolute value of the slope of this function, affecting the stability of fixed points of the system.

Significant dynamical differences arise as the infinite slope of the firing function at oscillation onset becomes finite, and the oscillation onset itself is smoothed out by the noise. For example, the oscillation in the firing rate at the onset of firing in the inhibitory case gives way to a constant firing rate if noise is assumed (see Figure 11). Also, the noise can decrease and even annihilate the range of input currents where bistability occurs in the excitatory case.

Such effects might also be caused by other currents known to smooth out firing functions (see, e.g., Ermentrout, 1998).

It is interesting to note that delayed feedback as in our model does produce some linearization of the frequency-input (f-I) characteristic in the inhibitory case (see Figure 3), as in Ermentrout's analysis (1998), even though the model here involves delays and total conductance increases (rather than an assumption that the main effect of the feedback/adaptation current is to shift the f-I curve—Ermentrout, 1998). However, our analysis of the deterministic model further predicts oscillations in a range around the onset of firing. This range is large if the feedback is strong. A full analysis of our model (and certain of its elaborations) in the context of linearization and gain control is forthcoming.

Our mathematical analysis is also substantiated by numerical simulations of an actual integrate-and-fire model with paired feedback. We have simulated the full spiking neuron, equation 2.1, with conductances governed by equations 2.19 through 2.26, and parameters as given in Table 1, and qualitatively reproduced all of the features of figures 1 and 3 (not shown). We used values of $\tau = 20$ and $a = 1/20$, which is equivalent after rescaling to the values $\tau = 1$, $a = 1$ used in the generation of those figures. We also produced apparently chaotic behavior using parameter values $\beta_e = 5.95$, $\beta_i = 1.05$, $I = 1$, $a = 1/10$, and $\tau = 80$ (equivalent after rescaling time to those used in Figure 7) (not shown). The value of f used in equations 2.22 and 2.26 was determined from the actual firing times of the neuron. The values $\tau = 20$ and $a = 1/20$ can be regarded as slow compared with the timescale of the spiking of the neuron, and it would be of interest to see how similar these timescales can be before the analysis presented here breaks down.

It would also be of interest to consider the inclusion of gating variables for the conductances on the dynamics of such paired feedback loops. Also, one could study the effect of other temporal properties of synapses such as depression and facilitation, which have been found, for example, in the loops of interest in weakly electric fish (John Lewis and Len Maler, personal communication, Jan. 2002). Another direction is to insert nonlinear functions of the firing function f used in the convolution integrals (see equations 2.5

and 2.6). Indeed, in certain systems, one of the pathways may not start firing (and thus modifying conductances) at the same level of activation as the other; in other words, the effect of different thresholds in the pathways is worth investigating. And possible multistability effects with respect to initial patterns of activation in the loop (Foss & Milton, 2000; Foss et al., 1996), which can arise specifically in delayed feedback systems when the delay distribution is sharp, could also be studied. It is worthwhile considering the activity of parallel arrays of such paired feedback loops, again suggested by the anatomy of many systems.

One can modify the noisy firing function to better mimic the effects of synaptic noise, which is a multiplicative noise in the dynamical equations, rather than an additive one, as considered here for simplicity. Note that while our study incorporated noise, it did so in a deterministic way by including the effect of noise in the firing function. This mimics the mean effects of noise. New effects are bound to arise, and new methods of numerical and bifurcation analysis are likely to be needed if the model dynamical equations are actually made stochastic. And, finally, perhaps novel computational properties will emerge as a consequence of making the variance of the synaptic noise dependent on the instantaneous rate of firing in the feedback pathways.

Acknowledgments

We thank John Lewis, Len Maler, Brent Doiron, John Milton, Michael Mackey, and Jacques Belair for useful discussions. This work was supported by NSERC (Canada), CIHR (Canada), and an Ontario Premiers Research Excellence Award.

References

an der Heiden, U. (1980). *Analysis of neural networks.* Berlin: Springer-Verlag.

Bastian, J. (1990). Descending control of electroreception. I. Properties of nucleus praeeminentialis neurons projecting indirectly to the electrosensory lateral line lobe. *J. Neurosci., 10*, 1226–1240.

Belair, J., Campbell, S. A., & van den Driessche, P. (1996). Frustration, stability, and delay-induced oscillations in a neural network model. *SIAM J. Appl. Math., 56*, 245–255.

Berman, N. J., & Maler, L. (1999). Neural architecture of the electrosensory lateral line lobe: Adaptations for coincidence detection, a sensory searchlight and frequency-dependent adaptive filtering. *J. Exp. Biol., 202*, 1243–1253.

Bressloff, P. C., & Coombes, S. (1999). Travelling waves in chains of pulse-coupled integrate-and-fire oscillators with distributed delays. *Physica D, 130*, 232–254.

Bressloff, P. C., & Coombes, S. (2000a). Dynamics of strongly coupled spiking neurons. *Neural Comput., 12*, 91–129.

Bressloff, P. C., & Coombes, S. (2000b). A dynamical theory of spike train transitions in networks of integrate-and-fire oscillators. *SIAM J. Appl. Math., 60*, 820–841.

Brunel, N. (1996). Hebbian learning of context in recurrent neural networks. *Neural Comput., 8*, 1677–1710.

Cajal, R. S. (1909). *Histologie du système nerveux de l'homme et des vertèbres*. Paris: Maloine.

Campbell, S. A. (1999). Stability and bifurcation in the harmonic oscillator with multiple, delayed feedback loops. *Dynam. Contin. Discrete Impuls. Systems, 5*, 225–235.

Contreras, D., Destexhe, A., Sejnowski, T. J., & Steriade, M. (1996). Control of spatiotemporal coherence of a thalamic oscillation by corticothalamic feedback. *Science, 274*, 771–774.

Crick, F., & Koch, C. (1998). Constraints on cortical and thalamic projections: The no-strong-loops hypothesis. *Nature, 391*, 245–250.

Dayan, P., & Abbott, L.F. (2001). *Theoretical neuroscience*. Cambridge, MA: MIT Press.

Destexhe, A. (1994). Oscillations, complex spatiotemporal behavior, and information transport in networks of excitatory and inhibitory neurons. *Phys. Rev. E, 50*, 1594–1606.

Diez-Martinez, O., & Segundo, J. P. (1983). Behavior of a single neuron in a recurrent inhibitory loop. *Biol. Cybern., 47*, 33–41.

Doiron, B., Chacron, M. J., Maler, L., Longtin, A., & Bastian, J. (2003). Inhibitory feedback required for network oscillatory responses to communication but not prey stimuli. *Nature, 421*, 539–543.

Douglas, R. J., Koch, C., Mahowald, M., Martin, K. A. C., & Suarez, H. H. (1995). Recurrent excitation in neocortical circuits. *Science, 269*, 981–985.

Engelborghs, K., Luzyanina, T., & Samaey, G. (2001). *DDE-BIFTOOL v. 2.00 user manual: A Matlab package for bifurcation analysis of delay differential equations* (Tech. Rep. TW-330). Department of Computer Science, K. U. Leuven, Belgium.

Ermentrout, G. B. (1994). Reduction of conductance-based models with slow synapses to neural nets. *Neural Comput., 6*, 679–695.

Ermentrout, B. (1998). Linearization by noise. *Neural Comput., 10*, 1721–1729.

Ermentrout, G. B., & Kopell, N. (1998). Fine structure of neural spiking and synchronization in the presence of conduction delays. *Proc. Natl. Acad. Sci. USA, 95*, 1259–1264.

Ermentrout, G.B., Pascal, M., & Gutkin, B. (2001). The effects of spike frequency adaptation and negative feedback on the synchronization of neural oscillators. *Neural Comput., 13*, 1285–1310.

Ernst, U., Pawelzik, K., & Geisel, T. (1995). Synchronization induced by temporal delays in pulse-coupled oscillators. *Phys. Rev. Lett., 74*, 1570–1573.

Eurich, C. W., Mackey, M. C., & Schwegler, H. (2002). Recurrent inhibitory dynamics: The role of state-dependent distributions of conduction delay times. *J. Theor. Biol., 216*, 31–50.

Fohlmeister, J. (1979). A theoretical study of neural adaptation and transient responses due to inhibitory feedback. *Bull. Math. Biol., 41*, 257–282.

Foss, J., Longtin, A., Mensour, B., & Milton, J. G. (1996). *Phys. Rev. Lett., 76,* 708–711.

Foss, J., & Milton, J. G. (2000). Multistability in recurrent neural loops arising from delay. *J. Neurophysiol., 84,* 975–985.

Giannakopoulos, F., & Zapp, A. (2001). Bifurcations in a planar system of differential delay equations modeling neural activity. *Physica D, 159,* 215–232.

Glass, L., & Mackey, M. C. (1988). *From clocks to chaos: The rhythms of life.* Princeton, NJ: Princeton University Press.

Glass, L., & Malta, C. P. (1990). Chaos in multilooped negative feedback systems. *J. Theor. Biol., 145,* 217–223.

Golomb, D., & Ermentrout, G. B. (2002). Slow excitation supports propagation of slow pulses in networks of excitatory and inhibitory populations. *Phys. Rev. E, 65,* 061911.

Guglielmi, N., & Hairer, E. (1999) Order stars and stability for delay differential equations. *Numer. Math., 83,* 371–383.

Guillouzic, S., L'Heureux, I., & Longtin, A. (2000). Rate processes in a delayed, stochastically driven, overdamped system. *Phys. Rev. E, 61,* 4906–4914.

Hahnloser, R. H. R., Sarpeshkar, R., Mahowald, M. A., Douglas, R. J., & Seung, H. S. (2000). Digital selection and analogue amplification in a cortex-inspired silicon circuit. *Nature, 405,* 947–951.

Hansel, D., & Mato, G. (2001). Existence and stability of persistent states in large neuronal networks. *Phys. Rev. Lett., 86,* 4175–4178.

Hansel, D., & Sompolinsky, H. (1992). Synchronization and computation in a chaotic neural network. *Phys. Rev. Lett., 68,* 718–721.

Hayes, N. D. (1950). Roots of the transcendental equation associated with a certain differential-difference equation. *J. London Math. Soc., 25,* 226–232.

Herz, A.V.M., Li, Z., & van Hemmen, J. L. (1991). Statistical mechanics of temporal association in neural networks with transmission delays. *Phys. Rev. Lett., 66,* 1370–1373.

Hohn, N., & Burkitt, A. N. (2001). Shot noise in the leaky integrate-and-fire neuron. *Phys. Rev. E, 63,* 031902.

Kistler, W.M. and van Hemmen, J.L. (1999). Delayed reverberation through time windows as a key to cerebellar function. *Biol. Cybern., 81,* 373–380.

Knight, B. W. (2000). Dynamics of encoding in neuron populations: Some general mathematical features. *Neural Comput., 12,* 473–518.

Koch, C. (1999). *Biophysics of computation.* New York: Oxford University Press.

Kunysz, A. M., Shrier, A., & Glass, L. (1997). Bursting behavior during fixed–delay stimulation of spontaneously beating chick heart cell aggregates. *Am. J. Physiol., 273,* C331–C346.

Lansky, P., & Sacerdote, L. (2001). The Ornstein-Uhlenbeck neuronal model with signal-dependent noise. *Phys. Lett. A, 285,* 132–140.

Latham, P. E., Richmond, B. J., Nelson, P. G., & Nirenberg, S. (2000). Intrinsic dynamics in neuronal networks. I. Theory. *J. Neurophysiol., 83,* 808–827.

Longtin, A., & Milton, J. G. (1988). Complex oscillations in the human pupil light reflex with mixed delayed feedback. *Math. Biosc., 90,* 184–199.

Longtin, A., & Milton, J. G. (1989). Modelling autonomous oscillations in the human light reflex using non-linear delay-differential equations. *Bull. Math. Biol., 51*, 605–624.
Mackey, M. C., & Glass, L. (1977). Oscillations and chaos in physiological control systems. *Science, 197*, 287–289.
Mackey, M. C., & an der Heiden, U. (1982). The dynamics of recurrent inhibition. *J. Math. Biol., 19*, 211–225.
Markus, C., & Westerwelt, R. (1989). Stability of analog neural networks with delay. *Phys. Rev. A, 39*, 347–359.
Mensour, B., & Longtin, A. (1998). Power spectra and dynamical invariants for delay-differential and difference equations. *Physica, 113*, 1–25.
Murphy, P. C., Duckett, S. G., & Sillito, A. M. (1999). Feedback connections to the lateral geniculate nucleus and cortical response properties. *Science, 286*, 1552–1554.
Nelson, M. E. (1994). A mechanism for neuronal gain control by descending pathways. *Neural Comput., 6*, 242–254.
Pakdaman, K., Vibert, J. F., Boussard, E., & Azmy, N. (1996). Single neuron with recurrent excitation: Effect of the transmission delay. *Neural Networks, 9*, 797–818.
Plant, R. E. (1981). A FitzHugh differential-difference equation modeling recurrent neural feedback. *SIAM J. Appl. Math., 40*, 150.
Ricciardi, L. M. (1977). *Diffusion processes and related topics in biology*. Berlin: Springer-Verlag.
Seung, H. S., Lee, D. D., Reis, B. Y., & Tank, D. W. (2000). The autapse: A simple illustration of short-term analog memory storage by tuned synaptic feedback. *J. Comput. Neurosci., 9*, 171–185.
Shampine, L. F., & Thompson, S. (2000). Solving DDEs with MATLAB. Available on-line: http://www.radford.edu/~thompson/webddes/.
Shayer, L. P., & Campbell, S. A. (2000). Stability, bifurcation, and multistability in a system of two coupled neurons with multiple time delays. *SIAM J. Appl. Math., 61*, 673–700.
Sompolinsky, H., & Kanter, I. (1986). Temporal association in asymmetric neural networks. *Phys. Rev. Lett., 57*, 2861–2864.
Stépán, G. (1989). *Retarded dynamical systems: Stability and characteristic functions*. Longman Scientific and Technical.
Stark, L. (1968). *Neurological control systems*. New York: Plenum Press.
Traub, R. D., & Miles, R. (1991). *Neural networks of the hippocampus*. Cambridge: Cambridge University Press.
Wang, X. J. (1999). Synaptic basis of cortical persistent activity: The importance of NMDA receptors to working memory *J. Neuroscience, 19*(21), 9587.
Wilson, H. R., & Cowan, J. D. (1972). Excitatory and inhibitory interactions in localized populations of model neurons. *Biophys. J., 12*, 1–24.

Received October 11, 2002; accepted May 5, 2003.